

NAVAL POSTGRADUATE SCHOOL

Monterey, California



THESIS

**PSPICE MODELLING AND PARAMETRIC STUDY OF
MICROBOLOMETER THERMAL DETECTORS**

by

Scott W. Stetson

June 2001

Thesis Advisor:
Co-advisor:

Gamani Karunasiri
D. Scott Davis

Approved for public release; distribution is unlimited.

20011116 161

REPORT DOCUMENTATION PAGE			<i>Form Approved OMB No. 0704-0188</i>	
Public reporting burden for this collection of information is estimated to average 1 hour per response, including the time for reviewing instruction, searching existing data sources, gathering and maintaining the data needed, and completing and reviewing the collection of information. Send comments regarding this burden estimate or any other aspect of this collection of information, including suggestions for reducing this burden, to Washington headquarters Services, Directorate for Information Operations and Reports, 1215 Jefferson Davis Highway, Suite 1204, Arlington, VA 22202-4302, and to the Office of Management and Budget, Paperwork Reduction Project (0704-0188) Washington DC 20503.				
1. AGENCY USE ONLY (Leave blank)		2. REPORT DATE June 2001	3. REPORT TYPE AND DATES COVERED Master's Thesis	
4. TITLE AND SUBTITLE: Title (Mix case letters) PSPICE Modeling and Parametric Study of Microbolometer Thermal Detectors			5. FUNDING NUMBERS	
6. AUTHOR(S) Stetson, Scott W.				
7. PERFORMING ORGANIZATION NAME(S) AND ADDRESS(ES) Naval Postgraduate School Monterey, CA 93943-5000			8. PERFORMING ORGANIZATION REPORT NUMBER	
9. SPONSORING / MONITORING AGENCY NAME(S) AND ADDRESS(ES) N/A			10. SPONSORING / MONITORING AGENCY REPORT NUMBER	
11. SUPPLEMENTARY NOTES The views expressed in this thesis are those of the author and do not reflect the official policy or position of the Department of Defense or the U.S. Government.				
12a. DISTRIBUTION / AVAILABILITY STATEMENT Approved for public release; distribution is unlimited			12b. DISTRIBUTION CODE	
13. ABSTRACT (maximum 200 words) The operation of a bolometer thermal sensor is analogous to that of a charging capacitor in a generic RC circuit. As such, circuits containing bolometers can be analyzed with standard circuit simulation programs such as PSPICE. This thesis deals with the development of a bolometer model by using PSPICE with the aid of Analogue Behavior Modeling (ABM) capability, which allows the user to program circuit components with basic mathematical functions. The predictions of the model were found to be in good agreement with the reported experimental data, which demonstrates the accuracy of the model. The model was used to design a self-heating compensated thermal sensor with enhanced signal integration capability to improve the signal-to-noise ratio. We believe the model can be used to analyze any circuit containing bolometers to optimize the performance.				
14. SUBJECT TERMS Microbolometers, thermal sensors			15. NUMBER OF PAGES 78	
			16. PRICE CODE	
17. SECURITY CLASSIFICATION OF REPORT Unclassified	18. SECURITY CLASSIFICATION OF THIS PAGE Unclassified	19. SECURITY CLASSIFICATION OF ABSTRACT Unclassified	20. LIMITATION OF ABSTRACT UL	

NSN 7540-01-280-5500

Standard Form 298 (Rev. 2-89)
Prescribed by ANSI Std. Z39-18

THIS PAGE INTENTIONALLY LEFT BLANK

Approved for public release; distribution is unlimited

**PSPICE MODELING AND PARAMETRIC STUDY OF MICROBOLOMETER
THERMAL DETECTORS**

Scott W. Stetson
Lieutenant, United States Navy
B.A., Duke University, 1994

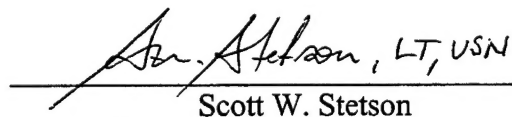
Submitted in partial fulfillment of the
requirements for the degree of

MASTER OF SCIENCE IN APPLIED PHYSICS

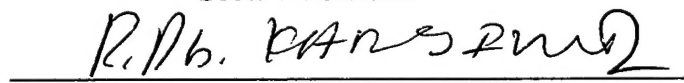
from the

**NAVAL POSTGRADUATE SCHOOL
June 2001**


Author:


Scott W. Stetson

Approved by:


Gamani Karunasiri, Thesis Advisor


David S. Davis, Second Reader


William B. Maier II, Chairman
Department of Physics

THIS PAGE INTENTIONALLY LEFT BLANK

ABSTRACT

The operation of a bolometer thermal sensor is analogous to that of a charging capacitor in a generic RC circuit. As such, circuits containing bolometers can be analyzed with standard circuit simulation programs such as PSPICE. This thesis deals with the development of a bolometer model by using PSPICE with the aid of Analogue Behavior Modeling (ABM) capability, which allows the user to program circuit components with basic mathematical functions. The predictions of the model were found to be in good agreement with the reported experimental data, which demonstrates the accuracy of the model. The model was used to design a self-heating compensated thermal sensor with enhanced signal integration capability to improve the signal-to-noise ratio. We believe the model can be used to analyze any circuit containing bolometers to optimize the performance.

THIS PAGE INTENTIONALLY LEFT BLANK

TABLE OF CONTENTS

TABLE OF CONTENTS	VII
LIST OF FIGURES	IX
I. INTRODUCTION.....	1
II. THEORY OF BOLOMETER OPERATION	5
A. GENERAL MODEL OF THERMAL DETECTORS.....	5
1. The Heat Transfer Equation.....	5
2. Steady-state Operation	6
3. Transient Operation	6
4. Practical Considerations and Trade-Offs.....	10
B. INTRODUCTION TO THE BOLOMETER	11
1. Description.....	11
2. Bolometer Design	12
C. READ-OUT CIRCUIT USING A WHEATSTONE BRIDGE.....	15
1. Purpose.....	15
2. Signal Voltage as a Function of Temperature Change.....	15
3. Power dissipated across bolometer.....	17
4. Wheatstone Bridge Response to Bias Voltage.....	18
5. Radiative Thermal Conductivity	21
6. Figures of Merit.....	23
7. Measuring Incident Infrared Radiation	23
8. Compensating Bolometer Operations	26
III. MODELING THE BOLOMETER WITH PSPICE.....	31
A. DISCUSSION OF PSPICE	31
1. Bolometer Heat Transfer Equation versus the Parallel RC Circuit	31
B. THE SINGLE BOLOMETER WHEATSTONE BRIDGE	33
1. PSPICE Model of Single Bolometer Wheatstone Bridge	33
2. Verification of the PSPICE Model and Early Comparison with the Analytic Model.....	34
3. Verification of the Model by Comparison with Physical Data	38
4. Modeling the Compensating Bolometer Wheatstone Bridge and Final Verification.....	42
C. PARAMETRIC STUDY USING THE WHEATSTONE BRIDGE MODEL	46
1. Integration Time versus Noise Bandwidth	46
2. Application: Thermal Imaging Device.....	47
3. Further Possible Benefit – Cancellation by Integration.....	50
IV. CONCLUSION	57
APPENDIX A: THE BOLOMETER ARRAY.....	59

LIST OF REFERENCES.....	61
INITIAL DISTRIBUTION LIST.....	63

LIST OF FIGURES

Figure II.1	Thermal detector model.....	5
Figure II.2	RC parallel circuit.....	7
Figure II.3	General thermal detector step response.....	9
Figure II.4	Photographs of a low thermal conductance microbolometer (left) and a high thermal conductance microbolometer (right).....	12
Figure II.5	Microbolometer pixel design.....	13
Figure II.6	Scanning electron microscope (SEM) image of a microbolometer showing the etches along the 111 plane.....	14
Figure II.7	Images taken by a microbolometer FPA under increasing vacuum of values 1) ambient pressure 2) 100 torr 3) 5 torr 4) 1×10^{-4} torr.....	14
Figure II.8	Wheatstone bridge with one bolometer. In the text, V_{Bias} will be denoted by V_b and ΔV_{out} will be denoted by V_{out}	15
Figure II.9	Output voltage for a one-bolometer Wheatstone bridge with $G = 3.2 \times 10^{-7} W/K$, $H = 4 \times 10^8 J/K$, $R = 16 K\Omega$, and $\alpha = 0.27\%$	19
Figure II.10	Depiction of the output voltage response for Wheatstone bridge over a period of time $t \ll \tau$	20
Figure II.11	Exaggerated illustration of the output voltage to due Joule heating alone and to Joule heating combined with incident IR.....	24
Figure II.12	Compensating bolometer Wheatstone bridge circuit.....	25
Figure II.13	Temperature responses of a sensor bolometer and reference bolometer. The upper curve represents B_1 and the lower curve represents B_2 , where $G_2 = 2G_1$	26
Figure II.14	Scale view of response in which applied power = $1000 \times IR$ power and $G_2 = 2 \times G_1$. The right hand figure illustrates the initial equivalent linear growth for both curves.....	28
Figure III.1	Virtual circuit representing a bolometer.....	32
Figure III.2	PSpice model of Wheatstone bridge with a single bolometer.....	33
Figure III.3	Joule heating power dissipated for varying bias voltages.....	35
Figure III.4	Effects of increasing temperature on dissipated power.....	37
Figure III.5	Experimental output voltages for the two bolometers as a function of time at 294 K (Ramakrishna, <i>et al</i>).....	39
Figure III.6	Simulated output voltage for bolometer B_1 and bolometer B_2 at 294 °K....	39
Figure III.7	PSpice simulated temperature change for bolometer B_1	40
Figure III.8	Physical data for bolometer B_1 (left) and bolometer B_2	41
Figure III.9	PSpice simulation of bolometer response to incident IR in addition to Joule heating. Bolometer B_1 is represented by the left graph, bolometer B_2 by the right graph.....	42
Figure III.10	IR and Joule heating response of the bridge consisting of two bolometers contrasted with response of the bolometer B_1 at bias voltage of 3V. The two bolometers were exposed to the same amount of infrared from a blackbody source.....	43

Figure III.11	PSPICE simulation of the IR and Joule heating response of the bridge consisting of two bolometers contrasted with response of the bolometer B_1 at bias voltage of 3V. The two bolometers were exposed to the same amount of simulated infrared flux from a blackbody source.....	44
Figure III.12	Compensated bolometer Wheatstone bridge.....	45
Figure III.13	Comparison of integration times with and without a compensating bolometer.....	49
Figure III.14	Unbalanced Wheatstone bridge.....	51
Figure III.15	PSPICE simulated output voltage versus time for integration by cancellation design.....	52
Figure III.16	Wheatstone bridge with voltage noise source for lower right resistor.....	53
Figure A.1	Microbolometer Focal Plane Array (FPA) architecture.....	59

I. INTRODUCTION

Infrared (IR) technology remains vital to military, law enforcement and fire-fighting applications. Numerous means of detecting IR radiation exist, each with its own drawbacks and advantages. Among these, for example, the HgCdTe and InSb-based photodetectors typically have superior performance and moderate cost, but they, as well as many others, require cooling to reduce dark current (Rogalski, 1994). This in turn requires a larger, heavier overall package and higher power consumption.

The need for small, lightweight, uncooled, sensitive IR devices has grown in particular in the military as a complement to the trend of smaller unit tactics and in response to the need for more intelligence and identification capability at the organic level. From imaging devices mounted on rifles to thermal detectors disguised as small plants providing perimeter surveillance, uncooled IR technology holds the promise of providing an edge over the enemy.

The *thermistor bolometer*, which we will refer to simply as the *bolometer*, is a temperature-variable resistor which can be used in uncooled systems. By measuring the change in resistance, a signal can be found which is dependent only on the change in temperature which the bolometer experiences due to incident IR flux. A number of difficulties have been overcome, such as vacuum-encapsulating the bolometer to eliminate unwanted conduction of heat from the sensor by surrounding air. Nevertheless, a large obstacle to high sensitivity remains: the signal itself is affected by the very act of measuring it.

To measure the change in resistance which has been caused by heating the bolometer, a bias voltage must be applied across it. The resulting current may then be

measured, and the change in resistance may be calculated. The difficulty in measuring the optically-induced change in resistance comes about because of the additional ohmic heating that the current generates. If we calculate the incident power due to a typical IR signal ($\sim \text{nW}$) versus this self-heating ($\sim \text{mW}$), also called *Joule* heating, we find that at detector saturation the Joule heating is typically three orders of magnitude higher than the IR signal.

The issue then becomes how to discriminate the signal from the self-heating response. In most applications, the self-heating response is first measured in the absence of an IR signal. This *dark current* value is then subtracted from subsequent measured signals. While this technique is relatively inexpensive and easily implemented, it is prone to error* and limits the dynamic range of the amplifying circuitry.

A more promising technique is the use of a reference bolometer, which, if incorporated into a Wheatstone bridge arrangement (see figure II.7), can theoretically cancel out the self-heating response if it is optically isolated from incident IR radiation. One method was introduced in a European patent (Kimura, *et al*, 1997), which provides a physical shield for the reference bolometer. This technique may be effective, but it is very costly when implemented into micro-machined bolometer circuits.

The necessity for low-cost, easily fabricated silicon chip technology prompted Karunasiri, *et al*, to investigate the possibility of rendering the reference bolometer translucent to IR by means of adjusting its thermal characteristics. Promising physical experiments validated this concept (Karunasiri, 1999), but it has not been fully explored.

* an average value is subtracted from the actual integrated signal value, for example.

Analytical models of the process can be derived using first-order approximations, but what was needed next was a suitable computer model that could account for higher-order effects in order to further refine the concept of manipulating the reference bolometer's thermal characteristics to improve self-heating cancellation.

The purpose of this thesis is to develop a tool to conduct parametric studies of bolometer operation. What follows is the development of such a model using PSPICE, an industry-standard electrical engineering circuit analysis tool. PSPICE is used in a novel way to simulate the thermal characteristics of the bolometer. The model is verified against physical experimental data, and then an example is given of how the model can be used to explore and refine the concept of self-heating cancellation through the use of a compensating bolometer.

THIS PAGE INTENTIONALLY LEFT BLANK

II. THEORY OF BOLOMETER OPERATION

A. GENERAL MODEL OF THERMAL DETECTORS

1. The Heat Transfer Equation

The operation of a generalized thermal detector can be understood by using a commonly accepted model wherein the sensor element is connected to a heat sink. Energy absorbed by the sensor is transported via a bridge with *thermal conductance* G to the heat sink. From the heat sink, the energy is either removed by a thermo-electrical (TE) cooling process or it dissipates as the heat sink re-establishes thermal equilibrium with its environment.

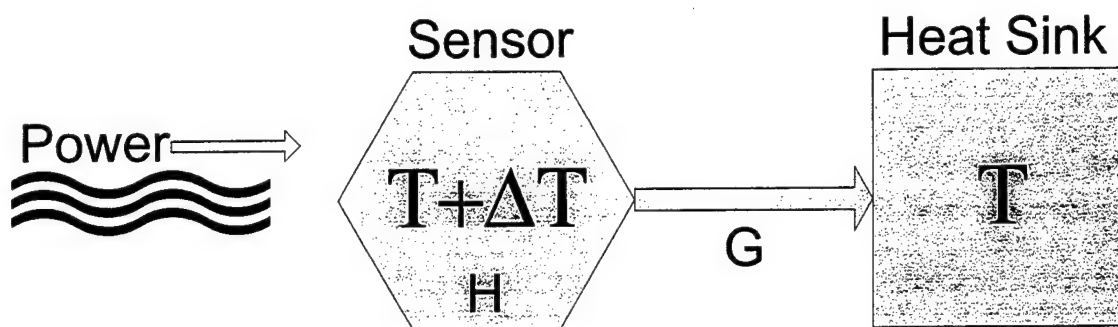


Figure II.1 Thermal detector model.

A natural trade-off exists between the signal response level of the sensor and how quickly the sensor can acquire a new signal; both are dependent on characteristics of the sensor material as well as the physical connection to the heat sink. The process described here is governed by the *heat transfer equation*, which is given by (Boreman, Dereniak, 1996)

$$P_{incident} = G \cdot \Delta T + H \frac{d\Delta T}{dt}. \quad (II.1)$$

The heat transfer equation, which is a statement of energy conservation, states that the incident power ($P_{incident}$) equals the thermal conductance (G) times the change in temperature, plus the heat capacity (H) times the rate of change of temperature. Thermal conductance, not surprisingly, is the ability of a device to conduct thermal energy and has units of watts per kelvin (W/K). Heat capacity (H) is the ability of a device to accept thermal energy in the form of heat and has units of joules per kelvin (J/K). Typical values of G and H for a microbolometer are 10^{-7} W/K and 10^{-9} J/K, respectively.

2. Steady-state Operation

Assuming a scenario wherein the sensor is subject to a constant incident radiative power flux, the sensor will reach a certain maximum temperature as its heat capacity is filled up. At this point the incident power simply passes through the sensor to the heat sink where it is dissipated. This change in temperature can be extracted from the heat transfer equation by setting the rate of temperature change equal to zero and solving for ΔT .

When $d\Delta T/dt = 0$,

$$\Delta T = \frac{P}{G}. \quad (II.2)$$

3. Transient Operation

Given the governing heat transfer differential equation $H \frac{d\Delta T}{dt} = P - G \cdot \Delta T$, we wish to solve for the function ΔT in order to understand the bolometer's change of

temperature as a function of time during the transient stages. Comparing the heat transfer equation to the equation governing the charging of a capacitor in a simple RC circuit with a constant current source I , note the similarity:

$$H \frac{d\Delta T}{dt} + G \cdot \Delta T = P \quad \text{versus} \quad C \frac{dV}{dt} + \frac{V}{R} = I. \quad (\text{II.3})$$

The RC circuit which equation (II.3) describes is shown below.

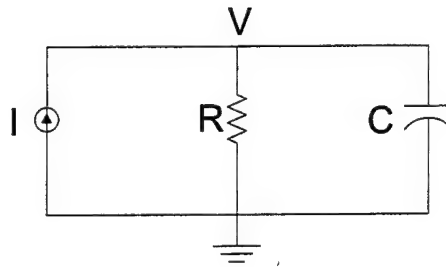


Figure II.2 RC parallel circuit

The solution to the RC circuit, assuming the initial value $V=0$ at $t=0$, is $V = IR(1 - e^{-t/RC})$, and by comparison we should expect a similar solution to the heat transfer equation of the

form $\Delta T = \frac{P}{G}(1 - e^{-tG/H})$ if $\Delta T=0$ at $t=0$:

Rearranging the heat transfer equation,

$$\frac{d\Delta T}{G\Delta T - P} = \frac{-dt}{H}.$$

Let $y = G\Delta T - P$ and $dy = Gd\Delta T$. Then,

$$\frac{dy/G}{y} = \frac{-dt}{H}.$$

Moving G to the right side and integrating both sides,

$$\int \frac{dy}{y} = - \int \frac{dt}{H/G}.$$

Assigning $H/G = \tau$, the time constant,

$$\ln(y) = -\frac{t}{\tau} + c, \text{ where } c \text{ is an arbitrary constant.}$$

To solve for the constant of integration, we apply the boundary condition that at $t = 0$ the change in temperature (ΔT) also equals zero, and hence $y = -P$ (from $y = G\Delta T - P$):

$$\ln(-P) = c, \text{ and therefore } \ln(y) = -\frac{t}{\tau} + \ln(-P).$$

Collecting terms,

$$\ln\left(\frac{y}{-P}\right) = -\frac{t}{\tau},$$

and solving for y yields

$$y = -Pe^{-t/\tau}.$$

Substituting the original value of $y = G\Delta T - P$ we arrive at

$$G\Delta T - P = -Pe^{-t/\tau},$$

and finally

$$\Delta T = \frac{P}{G} \left(1 - e^{-t/\tau}\right), \text{ where } \tau = H/G. \quad (\text{II.4})$$

Typical values of τ are on the order of 10^{-3} seconds⁻¹ and are obviously material and design specific.

If the incident radiation is removed after the sensor reaches saturation, $P = 0$, and we may observe how the device cools:

$$0 = G \cdot \Delta T + H(d\Delta T/dt).$$

Rearranging,

$$\frac{d\Delta T}{G\Delta T} = \frac{-dt}{H},$$

and

$$\frac{dy/G}{y} = \frac{-dt}{H},$$

substituting $y = G\Delta T$ this time,

$$\Delta T = -\frac{P}{G} e^{-t/\tau}, \quad (\text{II.5})$$

where P is the power used to achieve the steady state from which the temperature then falls. The following figure illustrates the relationship between the change in temperature and the application of constant power which is then “turned off” instantaneously (step response).

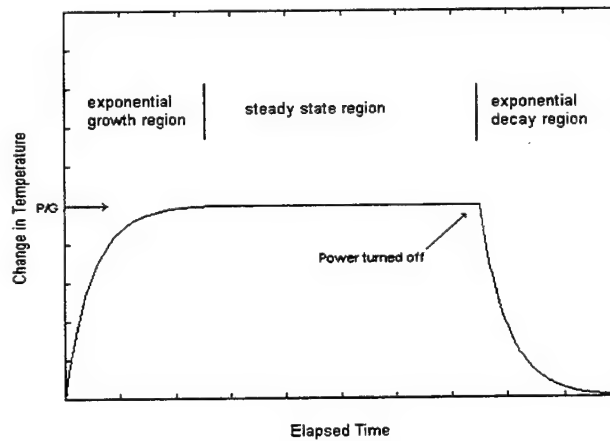


Figure II.3 General thermal detector step response.

4. Practical Considerations and Trade-Offs

As equation II.1 shows, a bolometer measures incident power by changing its temperature. The physical parameter that is actually measured is the temperature change ΔT . A value for P may then be extracted by applying equation (II.2), assuming G and H are known quantities. The other assumption made here is that we are measuring ΔT once the sensor has reached its steady state. Otherwise, as figure II.2 illustrates, we measure a time-dependent transient response akin to equation II.4, which is a more complicated function of P .

To describe how the sensor responds to incident IR, we define the *temperature responsivity* of the detector by

$$R_T = \frac{\Delta T}{P}. \quad (\text{II.6})$$

Noting that $\Delta T = P/G$ for steady-state conditions [equation (II.2)], we may re-write equation (II.6) as

$$R_T = \frac{1}{G} \quad (\text{II.7})$$

and we see that responsivity is inversely proportional to G .

Another important parameter for a detector is speed, or temporal frequency response. In the derivation of equation (II.4), we determined that the time constant $\tau = H/G$, where $\tau \approx 1/\Delta f$ and Δf is the effective frequency response bandwidth. Considering this and equation (II.7) we see that *speed and responsivity are inversely proportional*. One gives up frequency response for greater responsivity in thermal detectors. Indeed, it is evident that the responsivity-bandwidth product $R_T \Delta f$ is a constant for a bolometer of a given heat capacity.

B. INTRODUCTION TO THE BOLOMETER

1. Description

A bolometer is a device whose electrical resistance changes as a function of its temperature. Bolometers are also known as *thermistor* bolometers, or *thermally sensitive resistors*. The bolometer's ability to change resistance is described by its *temperature coefficient of resistance* (TCR), which will be hereafter denoted by α . Typical α values for metals material run in the region of approximately 0.3% change per degree celsius, but semiconductors may have values as high as 2% change per degree celsius. The value of α is used to determine resistance of a bolometer at a given temperature as:

$$R(T) = R_0(1 + \alpha \cdot [T - T_0]), \quad (\text{II.8})$$

where R_0 is the bolometer's resistance at ambient conditions, T_0 is the ambient temperature and T is the instantaneous bolometer temperature. ($T - T_0$ will be designated by ΔT hereafter.)

A microbolometer is simply a miniature bolometer micro-machined or photo-etched onto a substrate, typically silicon. Figure II.4 shows a pair of microbolometer images.

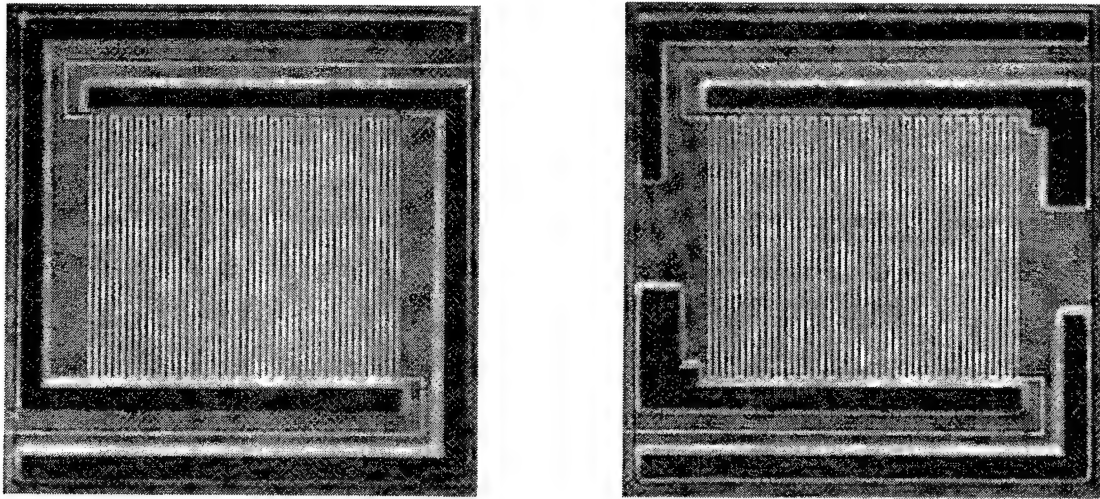


Figure II.4 Photographs of a low thermal conductance microbolometer (left) and a high thermal conductance microbolometer (right). (Ramakrishna, *et al*, 1999)

The bolometers shown above are identical in every way with the notable exception being the addition of two wide connections to the substrate heat sink on the right bolometer. These additional bridges provide more material through which heat may flow to the heat sink. Hence, the right bolometer has a higher thermal conductance.

2. Bolometer Design

From both engineering and economical points of view, it is of great importance that the entire sensor be designed to fit onto a single silicon chip as an integrated circuit. Attempting to attach leads to individual circuit elements will otherwise dramatically reduce the manufacturing yield and increase the cost per detector. A cursory look at the micromachining process of a bolometer may provide a more thorough understanding of its physical characteristics. Figure II.5 (below) depicts a typical design.

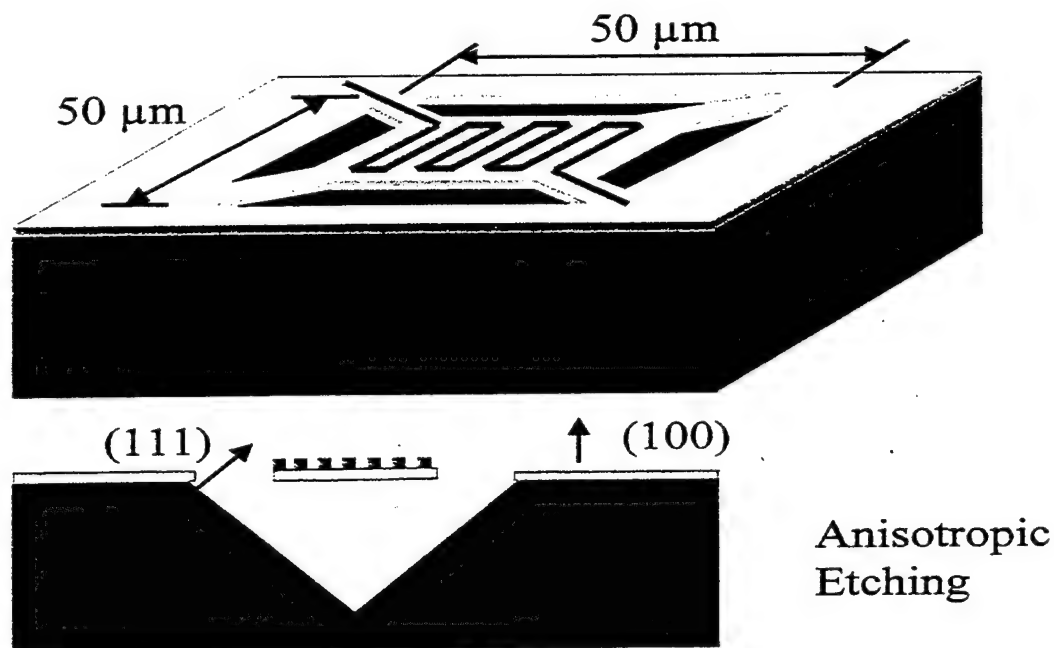


Figure II.5 Microbolometer pixel design.

The surface features are etched using standard lithographic processes. In order to thermally isolate the bolometer (with the exception of its bridges to the heat sink), the region below the bolometer is etched, for example, using tetramethyl ammonium hydroxide (TMAH) solution. This solution interacts with the p-type (100) silicon substrate in a useful fashion: it only etches the silicon in the 111 crystal plane direction. These 111 planes can be clearly seen in the following scanning electron microscope photograph (figure II.6). During measurement the device is placed under vacuum to eliminate any convective heat transfer. The importance of vacuum encapsulating the bolometer is demonstrated in figure II.7, which is a series of images taken by a focal plane array of bolometer pixels as it is placed under increasing vacuum. The image quality is improved because the bolometers suffer from increasingly less convection heat loss under increasing vacuum conditions.

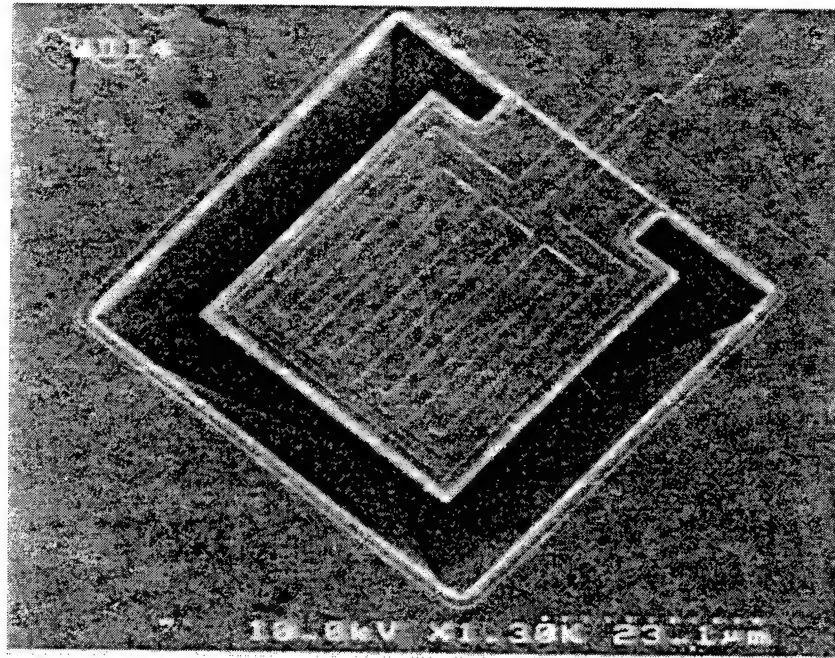


Figure II.6 Scanning electron microscope (SEM) image of a microbolometer showing the etches along the 111 plane. (Gu, *et al*, 1998)

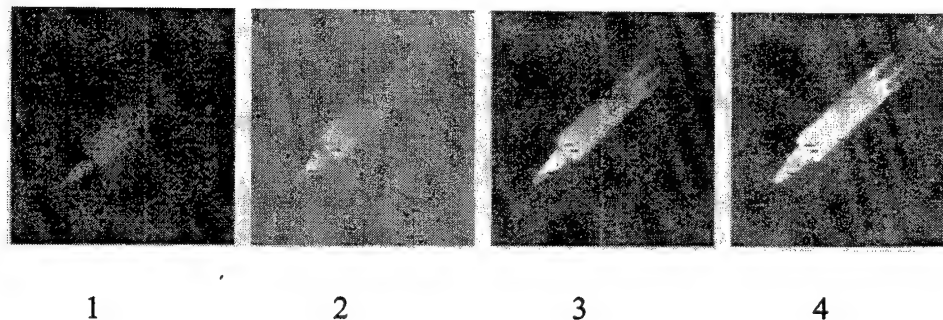


Figure II.7 Images taken by a microbolometer FPA under increasing vacuum of values 1) ambient pressure 2) 100 torr 3) 5 torr 4) 1×10^{-4} torr. (He, *et al*, 2000)

C. READ-OUT CIRCUIT USING A WHEATSTONE BRIDGE

1. Purpose

The Wheatstone bridge (Dereniak, 1996) is commonly used for isolating circuit components and making measurements on them. As a first step in employing a bolometer to measure temperature or infrared radiation (IR), the Wheatstone bridge provides a convenient circuit architecture. As will be discussed in section C.7, using a second bolometer for compensation improves the output signal, but for now it is instructive to look at a Wheatstone bridge with a single bolometer element in it, as depicted below.

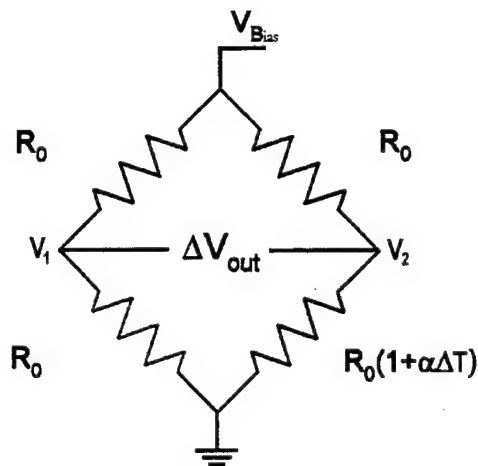


Figure II.8 Wheatstone bridge with one bolometer. In the text, V_{Bias} will be denoted by V_b and ΔV_{out} will be denoted by V_{out}

2. Signal Voltage as a Function of Temperature Change

As previously stated, the bolometer's resistance changes as a function of temperature in the following manner: $R(T) = R_0(1+\alpha\Delta T)$. Provided that no current flows through the nodes connecting V_1 and V_2 , we may consider both sides of the Wheatstone

bridge as voltage dividers with a bias voltage (V_b) applied, in which case the voltages with respect to ground may be calculated as follows.

$$V_1 = \frac{R_0}{2R_0} V_b, \quad V_2 = \frac{R(T)}{R_0 + R(T)} V_b. \quad (\text{II.9})$$

In an actual circuit we may measure the voltage across the bridge (V_{out}), which can be calculated as

$$V_{out} = V_1 - V_2 = V_b \left[\frac{R_0(1 + \alpha\Delta T)}{R_0 + R_0(1 + \alpha\Delta T)} - \frac{1}{2} \right] \quad (\text{II.10})$$

$$V_{out} = V_b \left[\frac{1 + \alpha\Delta T}{2 + \alpha\Delta T} - \frac{1}{2} \right]$$

$$V_{out} = V_b \left[\frac{1 + \alpha\Delta T}{2 + \alpha\Delta T} \left(\frac{2 - \alpha\Delta T}{2 - \alpha\Delta T} \right) - \frac{1}{2} \right]$$

$$V_{out} = V_b \left[\frac{2 + \alpha\Delta T - \alpha^2\Delta T^2}{4 - \alpha^2\Delta T^2} - \frac{1}{2} \right]$$

where the quadratic terms may be considered negligible if $|\alpha\Delta T| \ll 1$. Then,

$$V_{out} = V_b \left[\frac{2 + \alpha\Delta T}{4} - \frac{1}{2} \right],$$

and finally we are left with a relatively simple expression for the signal voltage (V_{out}) in terms of the change in temperature:

$$V_{out} = V_b \left[\frac{\alpha\Delta T}{4} \right]. \quad (\text{II.11})$$

From equation (II.5) we understand that ΔT is an exponential in time with a linear dependence on incident power, which means that in the Wheatstone bridge, V_{out} is also an exponential with a linear dependence on power. Two forms of power influence the temperature of the bolometer. Incident power is due to the incident IR radiation, which is what we wish to measure. The other form is dissipated power due to the bias voltage, which is applied in order to pass current through the bolometer in order to measure its changed resistance.

3. Power dissipated across bolometer

We now wish to consider more carefully how the heating of the bolometer occurs due to an external bias voltage (V_{bias}). This is known as *Joule heating* or *self heating*. To calculate the quiescent power dissipated across the bolometer, we square the voltage across the bolometer and divide by its resistance:

$$P_{Joule} = \frac{V_2^2}{R(T)}, \text{ where } V_2 = \frac{R(T)}{R_0 + R(T)} V_b, \text{ and } R(T) = R_0(1 + \alpha\Delta T).$$

$$P_{Joule} = \frac{R(T)}{(R_0 + R(T))^2} V_b^2 = \frac{R_0(1 + \alpha\Delta T)}{R_0^2 + 2R_0(R_0(1 + \alpha\Delta T)) + (R_0(1 + \alpha\Delta T))^2} V_b^2$$

$$P_{Joule} = \frac{R_0(1 + \alpha\Delta T)}{4R_0^2 + 4R_0^2\alpha\Delta T + R_0^2\alpha^2\Delta T^2} V_b^2$$

Dividing through by R_0 and treating the quadratic term as negligible for $|\alpha\Delta T| \ll 4$,

$$P_{Joule} = \frac{V_b^2}{4R_0} \cdot \frac{1 + \alpha\Delta T}{1 + \alpha\Delta T}, \quad (\text{II.12})$$

and we see that the power dissipation due to Joule heating is independent of ΔT as long as $|\alpha\Delta T| \ll 4$:

$$P_{Joule} = \frac{V_b^2}{4R_0}. \quad (\text{II.13})$$

Once steady state has been reached, all of the incident power will move through the bolometer to the heat sink, as can be described by the following set of equations:

$$H \frac{d\Delta T}{dt} = P_{incident} - G\Delta T \quad \text{and in a steady state, } \frac{d\Delta T}{dt} = 0, \text{ so}$$

$$P_{incident} = G\Delta T. \quad (\text{II.14})$$

As previously stated, equation (II.13) expresses power dissipated by the bolometer due only to the bias voltage. In an application setting in which we wish to measure the incident IR radiation, we must recognize that the voltage response of the Wheatstone bridge will be due to the sum of the incident IR power and the dissipated power due to Joule heating.

4. Wheatstone Bridge Response to Bias Voltage

Before determining the effects of external radiation, it is instructive to look at the output voltage of the circuit as a function of time, due to an applied bias voltage alone.

Figure II.8. Given equations (II.11) and (II.5), we may now write

$$V_{out} = \frac{V_b \cdot \alpha}{4} \frac{P_{Joule}}{G} \left(1 - e^{-t/\tau}\right) \quad (\text{II.15})$$

where t is the time elapsed since the application of V_b . In the absence of incident radiation, total power dissipated by the bolometer is given by the equation

$$P_{Joule} = \frac{V_b^2}{4R_0}, \quad (II.16)$$

and therefore the output voltage of the Wheatstone bridge is

$$V_{out} = \frac{V_b^3 \cdot \alpha}{16 \cdot R_0 \cdot G} \left(1 - e^{-t/\tau}\right). \quad (II.17)$$

The response, not surprisingly, takes on the same graphical form as that of the exponential rise in temperature depicted in figure II.3. Let us look more closely by inserting some typical values into equation (II.17). Figure II.8 represents the output voltage of just such a circuit (parameter values are given in the figure caption).

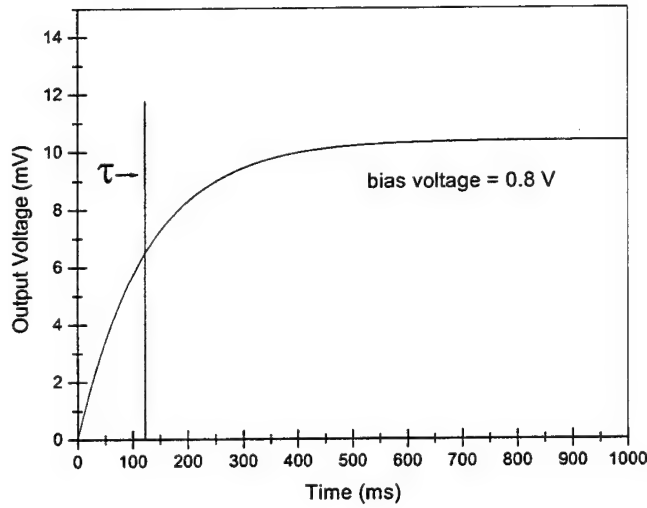


Figure II.9 Output voltage for a one-bolometer Wheatstone bridge with $G = 3.2 \times 10^{-7} W/K$, $H = 4 \times 10^8 J/K$, $R = 16 k\Omega$, and $\alpha = 0.27\%$.

For $t \gg \tau$ (steady state) the output voltage asymptotically approached the value of the prefix term in equation (II.17), which is called the *saturation voltage*

$$V_{saturation} = \frac{V_b^3 \cdot \alpha}{16 \cdot R_0 \cdot G} \quad (II.18)$$

and in the example of figure II.9 is calculated to be approximately 10.4 mV. Equation (II.18) may be used to determine the bolometer detector system's G from a measurement of $V_{saturation}$.

It is also useful to determine an empirical value for the system's H parameter. For $t \ll \tau$, we expand the exponential term to the first order and simplify:

$$V_{out} = \frac{V_b^3 \cdot \alpha}{16 \cdot R_0 \cdot G} \left(1 - \left(1 - \frac{t}{\tau} \right) \right)$$

$$V_{out} = \frac{V_b^3 \cdot \alpha}{16 \cdot R_0 \cdot G} \frac{t}{\tau},$$

and using equation II.4,

$$V_{out} = \frac{V_b^3 \cdot \alpha}{16 \cdot R_0 \cdot H} \cdot t. \quad (II.19)$$

From this equation we observe a linear response for small t which is independent of G . If we were to collect a number of data points for this time region, we would obtain a plot of the form found in figure II.10.

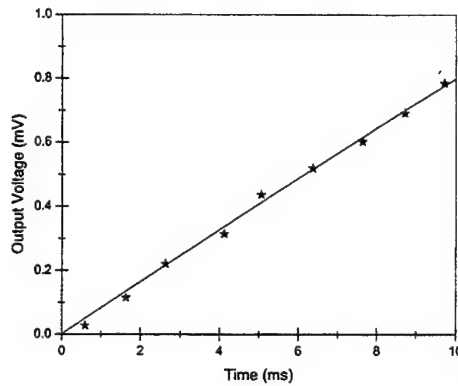


Figure II.10 Depiction of the output voltage response for Wheatstone bridge over a period of time $t \ll \tau$.

The fitted slope of the corresponds to the coefficient of t in equation (II.19), which can then be used to solve for H . Hence, one can determine both H and G with one set of measurements.

5. Radiative Thermal Conductivity

One important consideration should be noted, however, concerning thermal conductance. Heat transfer occurs in three forms: convection, conduction and radiation. With the bolometer under vacuum, convection is negligible. Nevertheless, while heat put into the bolometer will be conducted through the bridges attaching it to the heat sink, it may also radiate. When an object heats up, it radiates in accordance with the *Stefan-Boltzman Law* (Dereniak, 1996), which gives the radiant power as

$$P_{rad} = A\epsilon\sigma(T^4 - T_0^4), \quad (\text{II.20})$$

where T_0 is the ambient temperature, A is the radiant surface area, *emissivity* ϵ is a function of the bolometer material, and the *Stefan-Boltzman constant* $\sigma = 5.67 \times 10^{-8} \text{ watt}/(\text{m}^2 \cdot \text{K}^4)$. A true blackbody has an emissivity of exactly one. Considering that most metals are more reflective than emissive, one would assume our titanium bolometer would have a relatively low emissivity. Because the bolometer is typically biased with low voltages, it seems unlikely that emissivity would play a role at correspondingly small temperature changes (e.g. less than 100 K), but it certainly warrants analysis.

The question is whether or not enough power is radiated away from the bolometer ($P_{radiated}$) so as to make a significant impact on the measured signal. To help describe the radiative transfer of energy, we define thermal conductivity due to radiation G_{rad} as

$$G_{rad} = \frac{P_{radiated}}{\Delta T}, \quad (2.21)$$

with the understanding that it is not an actual physical parameter but rather a construct which can assist us in describing radiation in convenient terms. Substituting equation (II.20) for the radiant power into equation (2.21),

$$G_{rad}\Delta T = A\varepsilon\sigma(T^4 - T_0^4). \quad (II.22)$$

Substituting $T_0 + \Delta T$ for T , and moving a ΔT to the right side,

$$G_{rad} = \frac{A\varepsilon\sigma\left([T_0 + \Delta T]^4 - T_0^4\right)}{\Delta T}. \quad (II.23)$$

Assuming ΔT is small relative to T_0^* , all but the first order terms can be dropped in a Taylor expansion of $[T_0 + \Delta T]^4$:

$$[T_0 + \Delta T]^4 = T_0^4 \left[1 + \frac{\Delta T}{T_0}\right]^4 \quad (II.24)$$

After the expansion and dropping of higher-order terms,

$$[T_0 + \Delta T]^4 \approx T_0^4 \left[1 + \frac{4\Delta T}{T_0}\right]. \quad (II.25)$$

This approximation can be re-inserted into equation (II.23) to yield

$$G_{rad} = \frac{A\varepsilon\sigma\left(T_0^4 \left[1 + \frac{4\Delta T}{T_0} - 1\right]\right)}{\Delta T} \quad (II.26)$$

which results in

$$G_{rad} = 4A\varepsilon\sigma T_0^3. \quad (II.27)$$

This result surprised the author, but upon reflection it certainly makes sense. Every object at room temperature is radiating in accordance with the Stefan-Boltzman Law; a slight change in temperature will not have a major effect on that radiation. The fact that

* At low bias voltages, typical ΔT 's are around 30 °K, compared with room temperature of 300 °K.

with small temperature changes G_{rad} is constant is fortunate for those who wish to establish a model that includes it. The method described earlier for calculating G remains valid, with the understanding that $G = G_{conductive} + G_{radiative}$.

6. Figures of Merit

The figures of merit for a general thermal detector discussed in chapter II.A.1 may now be revised so as to describe the bolometer in a Wheatstone bridge circuit. We now define voltage responsivity as

$$R_V = \frac{V_{out}}{P_{incident}} \quad (II.28)$$

and from equation (II.2) we have

$$\Delta T = \frac{P_{incident}}{G}$$

for a saturated bolometer, which is what would be measured. Substituting equation (II.2) into equation (II.11), we have

$$V_{out} = \frac{V_b \cdot \alpha \cdot P_{incident}}{4 \cdot G} \quad (II.29)$$

and equation (II.28) becomes

$$R_V = \frac{V_b \cdot \alpha}{4 \cdot G} \left[\frac{V}{W} \right]. \quad (II.30)$$

Regarding speed, the same relationship holds true for the time constant τ , which, as given by equation (II.4), is $\tau = H/G$.

7. Measuring Incident Infrared Radiation

In practice, if we were using our single bolometer Wheatstone bridge circuit to make measurements, we would expose it to the IR radiation for a more than three time constants in order to achieve steady state, apply a bias voltage pulse and measure the output voltage. If we compared this output voltage data with that of an experiment in

which we just measured the output voltage without incident IR, we would see something like the figure given below.

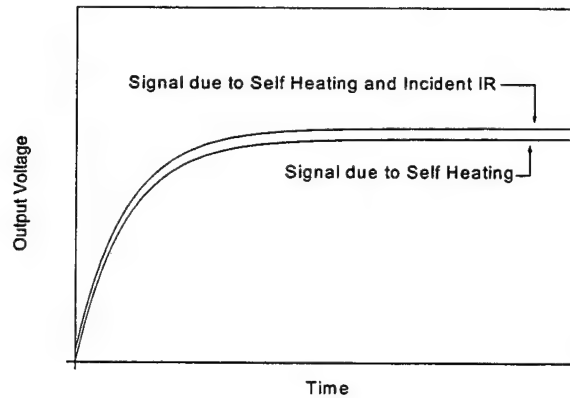


Figure II.11 Exaggerated illustration of the output voltage to due Joule heating alone and to Joule heating combined with incident IR.

Figure II.11 illustrates the resultant relative output voltages and is only provided for pedagogical use. It is in fact a gross exaggeration; the difference between the two curves would not be discernable if the two curves could be drawn to scale. Typical values for incident IR fluxes are in the nanowatt (nW) range, compared to milliwatts (mW) due to Joule heating. In an actual circuit, the minuscule IR signal would have to be extracted from the Joule heating response *prior to amplification*. If it were not removed, introduction of the Joule heating signal into the amplifier would cause quick amplifier saturation.

One way to compensate is to electronically subtract a calculated value of the Joule heating voltage from the composite signal. This method is used with numerous current devices, but it relies on analytically derived values to be subtracted from the experimental composite IR signal and Joule heating signal. If the signal is integrated for a certain period of time in order to improve the S/N ratio, cancellation becomes even more

difficult since the self-heating signal increases with time (see equation II.20) until the steady state. Another way would be to physically cancel the unwanted voltage by using a compensating bolometer on the opposite side of the Wheatstone bridge, as illustrated in the following schematic:

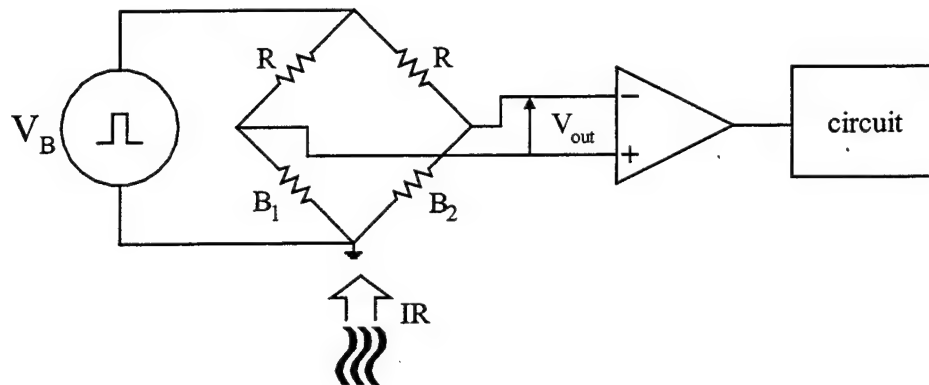


Figure II.12 Compensating bolometer Wheatstone bridge circuit.

In this arrangement either bolometer B_1 or bolometer B_2 is the “compensating” bolometer, which would mean that it should be optically masked from the incident IR radiation, but allowed to undergo normal Joule heating. With the objective of creating a micro-machined, integrated circuit on a silicon substrate, physically shielding the compensating bolometer from the IR radiation becomes impractical. However, by altering the thermal characteristics of the compensating bolometer, it can be made to appear virtually translucent to the IR irradiation. Specifically, by increasing its thermal conductivity, i.e. making the legs which attach the bolometer face to the heat sink larger, the energy which is absorbed will pass through the bolometer’s legs to the heat sink at a higher rate.

8. Compensating Bolometer Operations

The use of a compensating bolometer with higher thermal conductivity, as opposed to an identical bolometer which is physically shielded from incident IR flux, introduces a host of dynamic changes to the operation of the Wheatstone bridge. Changes in signal strength as well as thermal time constants accompany any change in the thermal conductivity of the reference bolometer. Figure II.13 depicts the temperature changes experienced by a sensor bolometer B_1 (upper curve) and a reference bolometer B_2 (lower curve) as they are both exposed to incident IR flux and then to a bias voltage step function.

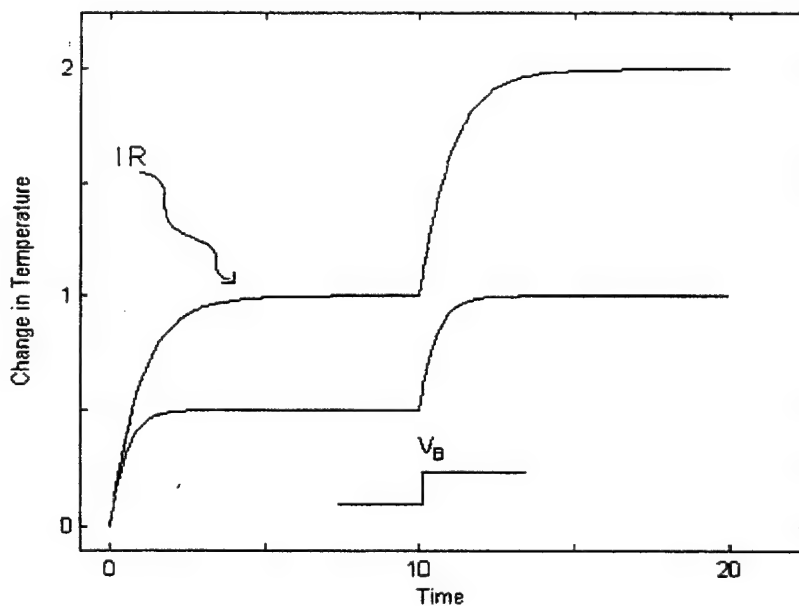


Figure II.13 Temperature responses of a sensor bolometer and reference bolometer. The upper curve represents B_1 and the lower curve represents B_2 , where $G_2=2G_1$.

In the interest of simplicity, incident IR power has been made equal to the power dissipated due to bias voltage. The thermal conductivity of the reference bolometer has

been arbitrarily selected to be twice that of the sensor bolometer, in order to demonstrate how thermal conductivity affects both the maximum signal strength and the speed with which the bolometer heats up, in accordance with equations (II.2) and (II.4), respectively:

$$\Delta T = \frac{P}{G}, \quad (\text{II.2})$$

$$\Delta T = \frac{P}{G} \left(1 - e^{-t/\tau} \right) \text{ where } \tau = H/G. \quad (\text{II.4})$$

The signal we wish to measure is the maximum temperature of the sensor bolometer due to incident IR flux, i.e., the upper curve before bias voltage is applied. With the reference bolometer in place, the actual IR signal available is the *difference* between the two curves before the bias voltage (ΔT). From this perspective, the reference bolometer has degraded the signal (by half). In practice, if we use a reference bolometer with a thermal conductivity one-tenth that of the sensor bolometer, we will experience only a 10% signal loss. Hence, the first of two design constraints is evident: *G_2 should be as large as possible to make B_2 optically transparent to IR radiation.*

The benefit of the reference bolometer becomes manifest when the bias pulse is applied and the two temperature levels rise exponentially. Considering the more realistic case in which Joule heating power is orders of magnitude higher than IR power, one might be tempted to wonder how an accurate signal can be extracted at all with the use of a reference bolometer. Analytic results in the case where $G_2=2G_1$ and dissipated power equals 1000 times incident IR power are given in the following figure, generated by MATLAB.

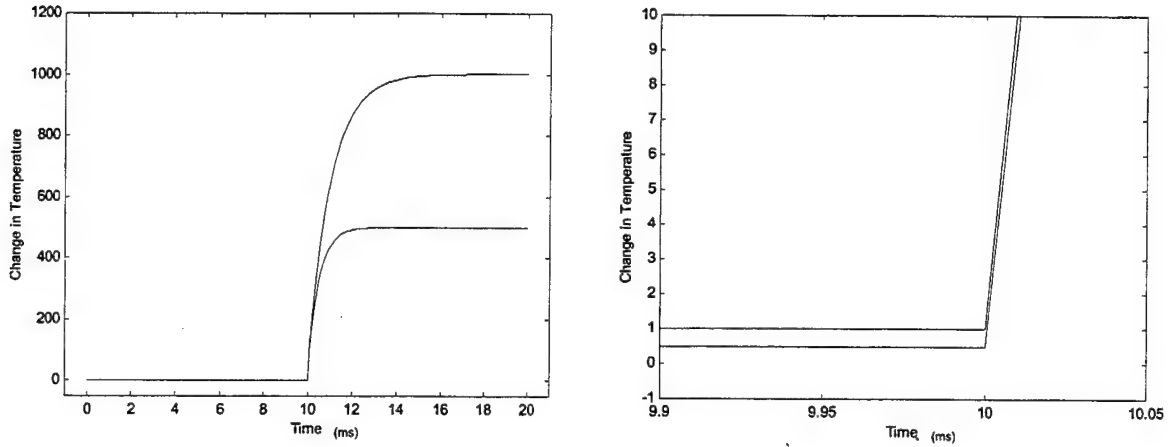


Figure II.14 Scale view of response in which applied power = $1000 \times \text{IR power}$ and $G_2 = 2 \times G_1$. The right hand figure illustrates the initial equivalent linear growth for both curves.

The original signal is completely buried shortly after bias voltage is applied for the read-out. Fortunately, while the temperatures of B_1 and B_2 grow with different exponential rates, there is a region in which their growth rates may be approximated as linear and independent of thermal conductance, which is illustrated in the right hand graph of Figure II.14. Rearranging the heat transfer equation,

$$d(\Delta T) = \frac{P}{H} dt - \frac{dt}{\tau} \Delta T. \quad (\text{II.31})$$

If $dt \ll \tau$, then equation (II.31) can be approximated as

$$d(\Delta T) \approx \frac{P}{H} dt. \quad (\text{II.32})$$

Therefore, in the region $dt \ll \tau$, where dt is the bias voltage pulse width, we should be able to integrate the signal to measure ΔT quite accurately, as long as the heat capacitances of the two bolometers are the same. Here we see our second design

constraint: *for τ to be large compared to dt , G_2 must be small*, so that it may heat up at the same rate as B_1 for at least long enough to obtain a read-out from integration.

These two competing design constraints were the motivation for a computer model that could be used to theoretically optimize various Wheatstone bridge configurations. With this in mind, Section III deals with developing and verifying an acceptable model using an industry-standard electrical engineering tool called PSPICE.

THIS PAGE INTENTIONALLY LEFT BLANK

III. MODELING THE BOLOMETER WITH PSPICE

A. DISCUSSION OF PSPICE

PSPICE is a computer simulation program that models the behavior of an electrical circuit containing analog devices. It is essentially a computer-based breadboard which allows one to predict AC and DC steady state and transient analyses. By using it to model the circuits described in Section II and then verifying the model against experimental data, we may confidently conduct parametric studies of the bolometer.

1. Bolometer Heat Transfer Equation versus the Parallel RC Circuit

As discussed in Section I, the heat transfer equation is of the same form as the differential equation for the parallel RC-circuit under constant current charging (Figure II.3.) The following are the two analogous equations:

$$\begin{aligned} P(t) &= G \cdot \Delta T + H \frac{d(\Delta T)}{dt} \quad (P(t) \text{ constant}) \\ I(t) &= \frac{1}{R} (V(t) - V_0) + C \frac{d(V(t))}{dt} \quad (I(t) \text{ constant}). \end{aligned} \tag{III.1}$$

Their analogous parameters are as follows, with their SI units in square brackets:

$$\begin{aligned} H \left[\frac{J}{K} \right] &\rightarrow C \left[\frac{A}{V} \right], \\ G \left[\frac{W}{K} \right] &\rightarrow \frac{1}{R} \left[\frac{1}{\Omega} \right], \\ T(t) [K] &\rightarrow V(t) [V], \\ P(t) [W] &\rightarrow I(t) [A]. \end{aligned} \tag{III.2}$$

Using this analogy, we can design a circuit using PSPICE to mimic the temperature-dependency of the bolometer's resistance. We can then insert this virtual circuit into

another circuit representing the actual Wheatstone bridge with a bias voltage applied to it. Special consideration must be given not to confuse the actual electric circuit values with the virtual “temperature circuit” values. The bolometer is modeled as an RC circuit with the resistor representing the thermal conductance and the capacitor representing heat capacity, as shown below.

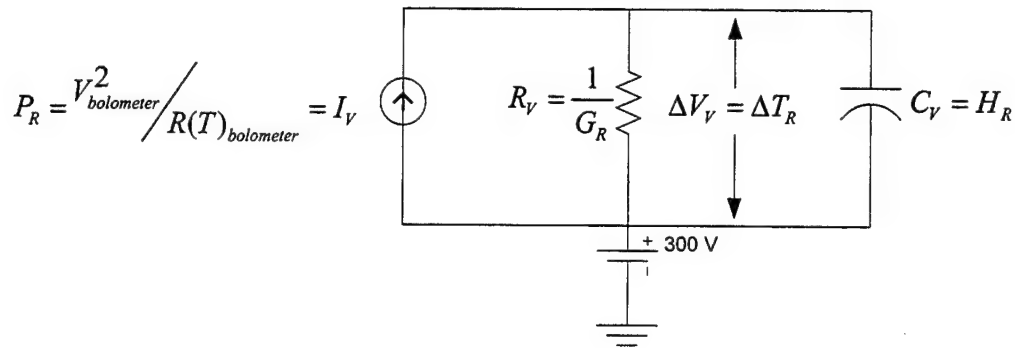


Figure III.1 Virtual circuit representing a bolometer.

Subscripts “R” and “V” stand for real and virtual quantities, respectively. $R(T)_{bolometer}$ is given by $R(T) = R_0(1 + \alpha \cdot \Delta T)$, and $V_{bolometer}$ is the value of the voltage drop across the bolometer in the Wheatstone bridge. The value of the current source in the virtual circuit corresponds to the power dissipated in the bolometer. In figure III.1, a voltage source maintains a virtual offset voltage of 300 V, placing the sensor’s initial temperature at room temperature conditions of 300 K. What remains is to connect the bolometer to a Wheatstone bridge and apply a bias voltage, all of which we can do using PSPICE.

B. THE SINGLE BOLOMETER WHEATSTONE BRIDGE

1. PSPICE Model of Single Bolometer Wheatstone Bridge

The point of interface for the circuit described above is the bolometer itself, represented by an analogue behavior modeling (ABM) box, which allows the user to control the output through the use of the algorithms he chooses. As there is no temperature-dependent resistor in the ABM options provided by PSPICE, we must replace the function of the resistor with an available option: a variable current source, which we can program to set the current through to be the same as that through the bolometer it replaces.

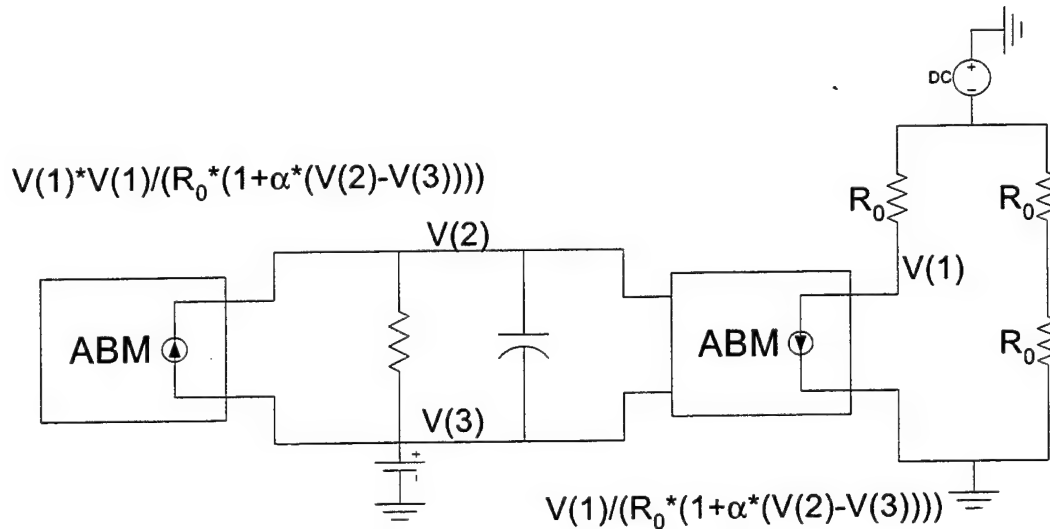


Figure III.2 PSPICE model of Wheatstone bridge with a single bolometer.

Figure III.2 represents the circuit as seen in the PSPICE format, with the exception being that the ABM formula accept only numeric values, as opposed to the formulas shown in the figure, which include α and R_0 to help clarify the figure. The ABM box receives temperature inputs $([V(2)-V(3)] \rightarrow \Delta T)$ from the virtual circuit to insert the correct

current into the Wheatstone bridge, acting as if there were a temperature-dependent resistor there. The current generated is given by

$$I(t) = \frac{V_{bolometer}}{R(T)}, \quad (III.3)$$

where $R(T)$ is

$$R(T) = R_0 (1 + \alpha \cdot \Delta T). \quad (III.4)$$

The virtual circuit is able to calculate the temperature difference ΔT by inserting the voltage drop across the bolometer in the actual circuit into an ABM box (far left) to generate a virtual power, whose RC-circuit analogue, according to equation (III.2), is current.

At this point the circuit has been designed to represent just the Joule heating effect without incident radiation. To include irradiance, a current source (analogous to power) would be placed in parallel with the resistor and capacitor in the bolometer circuit.

2. Verification of the PSPICE Model and Early Comparison with the Analytic Model

After creating the PSPICE model shown in figure III.2, the first step to verification is to observe the correlation of simulated data to the analytical predictions of Section II. One of the first experiments run was to verify equation (II.13), which states that the dissipated power in the bolometer is constant, given a steady bias voltage (V_b):

$$P_{Joule} = \frac{V_b^2}{4R_0}. \quad (II.13)$$

Recalling that a quadratic term of temperature ($R_0^2 \alpha^2 \Delta T^2$) was dropped from the denominator, what this simulation really seeks to determine is *for what region equation (II.13) is valid*. Using a bolometer with the same values as before ($G = 3.2 \times 10^{-7} \text{ W/K}$, $H = 4 \times 10^8 \text{ J/K}$, $R = 16 \text{ k}\Omega$, and $\alpha = 0.0027$), the results for applied bias voltages ranging from 1.0 to 10.0 volts are given below.

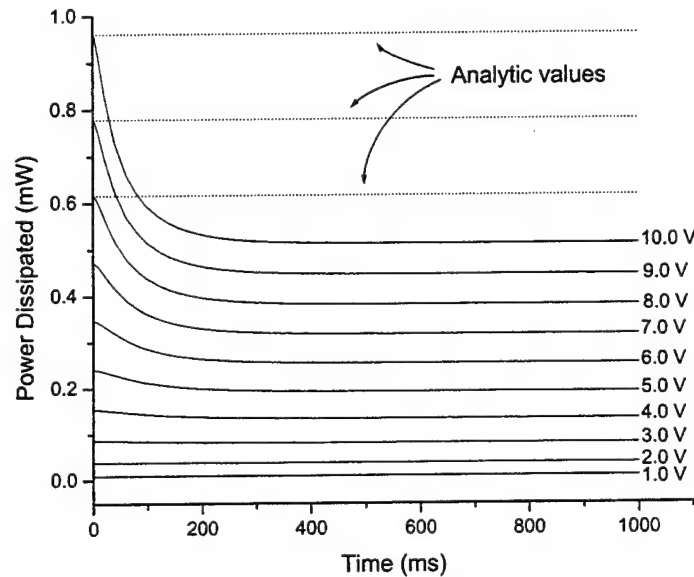


Figure III.3 Joule heating power dissipated for varying bias voltages.

Also shown are the corresponding analytical values for the top three bias voltages (8.0, 9.0, 10.0 V) as given by equation (II.13). What is quite apparent is the departure from the expected linear relationship. The nonlinear effects of the disregarded quadratic and higher temperature terms are in fact important. So what is the acceptable region of linearity?

We can determine the condition for acceptably disregarding the quadratic term in the equation

$$P = \frac{R_0(1 + \alpha\Delta T)}{4R_0^2 + 4R_0^2\alpha\Delta T + R_0^2\alpha^2\Delta T^2} V_b^2 \quad (\text{III.5})$$

by setting up the condition to be

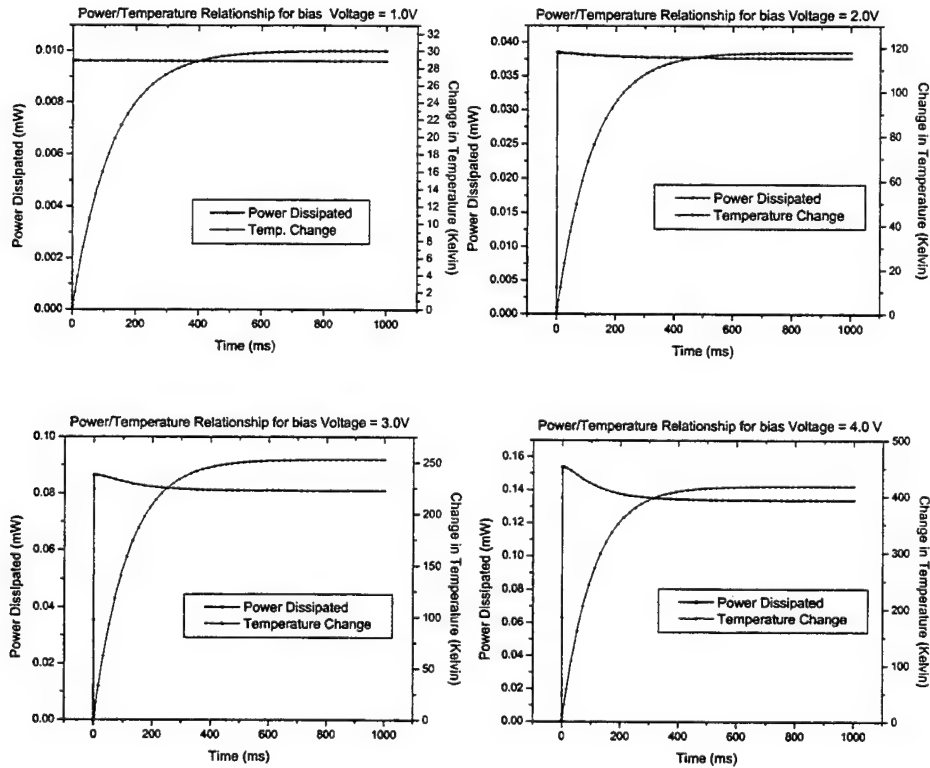
$$4R_0^2\alpha\Delta T \gg R_0^2\alpha^2\Delta T^2$$

which then leads to

$$\frac{4}{\alpha} \gg \Delta T. \quad (\text{III.6})$$

In the case of $\alpha=0.0027$ for Ti bolometers, the acceptable region must be $\Delta T \ll 1480$ K.

The exact region obviously depends upon how accurate a prediction one would like to make. The deterioration in linearity can clearly be seen in the following set of graphs.



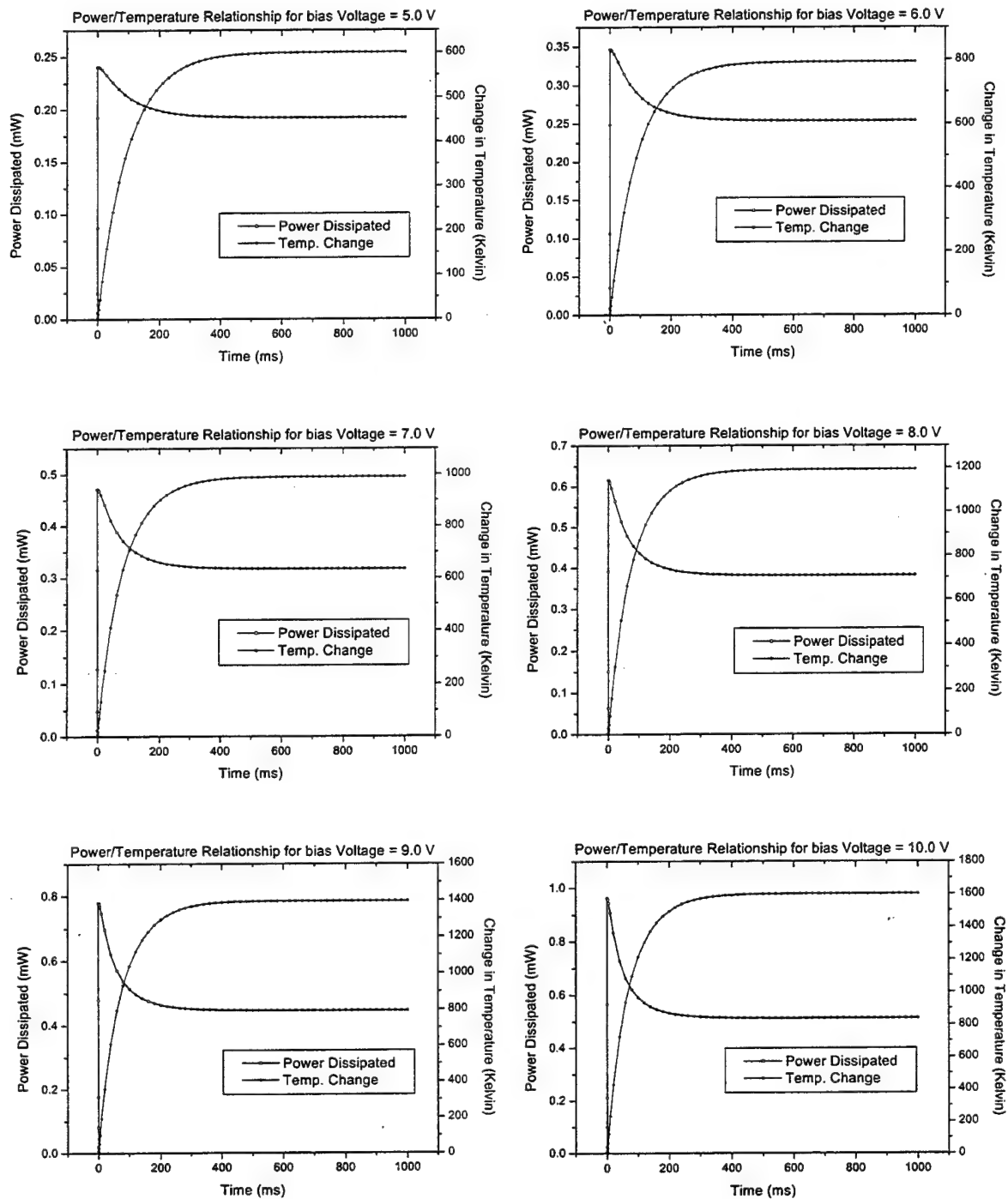


Figure III.4 Effects of increasing temperature on dissipated power.

One can actually begin to see degradation on the second graph ($V_b=2.0$ V), and by the fourth graph ($V_b=4.0$ V) there is significant deviation from the expected linear behavior. At $V_b=10.0$ V, the steady state power is slightly over *half* of the value predicted by the analytic model. By this point the temperature change is at approximately 1600 K. Hence we have clear verification that, in order for our model to be accurate, the bolometer must be operated in the region well below 1480 K, as equation (III.6) states.

3. Verification of the Model by Comparison with Physical Data

Having established the acceptable temperature regime, we can also verify the model by comparison with actual physical data (Ramakrishna, *et al*, 1999). Two bolometers with distinct thermal properties were used in a preliminary experiment to demonstrate the concept of a compensating bolometer Wheatstone bridge. The thermal characteristics are given in the following table.

	Bolomter B ₁	Bolomter B ₂
Resistance (at 294 K)	26 k Ω	24 k Ω
α (at 294 K)	0.0027/K	0.0029/K
Thermal Conductance (G)	3.61×10^{-7} W/K	2.37×10^{-6} W/K
Thermal Mass (H)	4.0×10^{-8} J/K	4.74×10^{-8} J/K
Thermal Time Constant (τ)	111 ms	15 ms
Responsivity (at 3 V)	6000 V/W	770 V/W

Table III.1 Bolometer characteristics

Below is a graph showing measured output voltage versus time for the two bolometers. Note that the upper and lower x-axes separately represent the two bolometers.

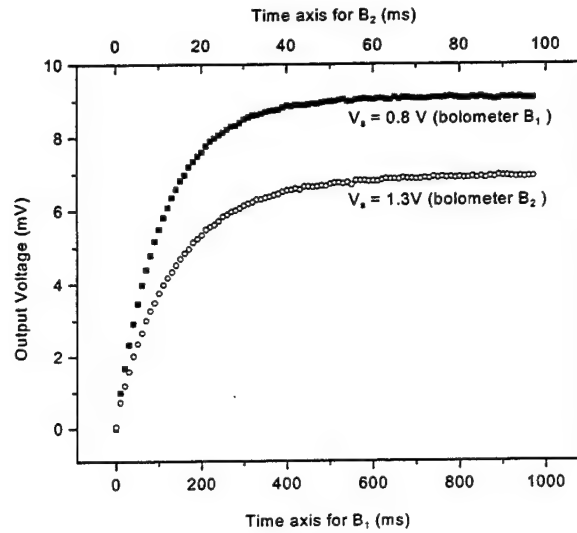


Figure III.5 Experimental output voltages for the two bolometers as a function of time at 294 K (Ramakrishna, *et al*).

Running a PSICE simulation with the same parameters, the following data is generated:

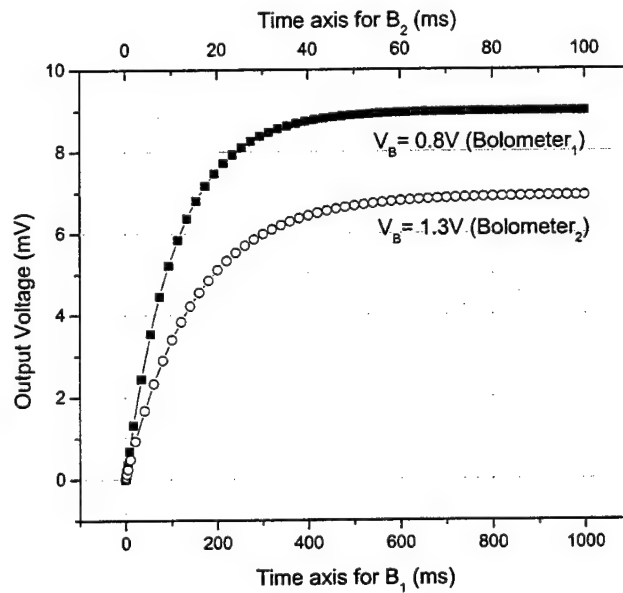


Figure III.6 Simulated output voltage for bolometer B₁ and bolometer B₂ at 294 °K.

The agreement between Ramakrishna and Karunasiri's physical experiment and the simulated experiment of figure III.6 falls within 1%. The data for figure III.6 is collected

in PSPICE by placing “voltage differential probes” on either side of the Wheatstone bridge, in each case between the two resistors, as shown in figure III.2. We can simulate monitoring the temperature by placing the voltage differential probes on the upper and lower branches of the bolometer’s virtual temperature circuit in figure III.2. Doing so yields the following data.

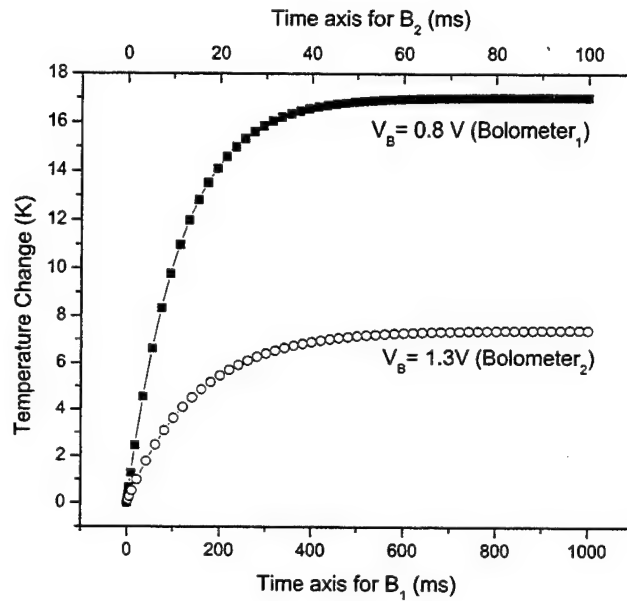


Figure III.7 PSPICE simulated temperature change for bolometer B₁

While it is not possible to measure the steady-state temperature change in the physical experiment, it can at least be calculated analytically to determine how closely the model agrees with analytic predictions. For bolometer B₁, with $V_{out} = 0.0091$ V, $V_b = 0.8$ V and $\alpha = 0.0027$ °K⁻¹, equation (II.11) yields $\Delta T = 16.85$ K. The PSPICE simulation yielded a maximum temperature change of 17.02 K, which indicates agreement within 1%. For bolometer B₂, with $V_{out} = 0.007$ V, $V_b = 1.3$ V and $\alpha = 0.0029$, equation (II.11) yields $\Delta T =$

7.427 K. In this case the PSPICE simulation generated a steady-state temperature change of 7.416 K, well under a 1% discrepancy. It should be noted that these slight errors may be due to estimating the saturation voltages from figure III.6, as actual numerical data was not available from the physical experiment.

Before completing the compensating bolometer Wheatstone bridge, we can compare modeled data with the physical data on how the individual bolometers respond to Joule heating and incident IR in the $dt \ll \tau$ region, where dt is the bias pulse width.

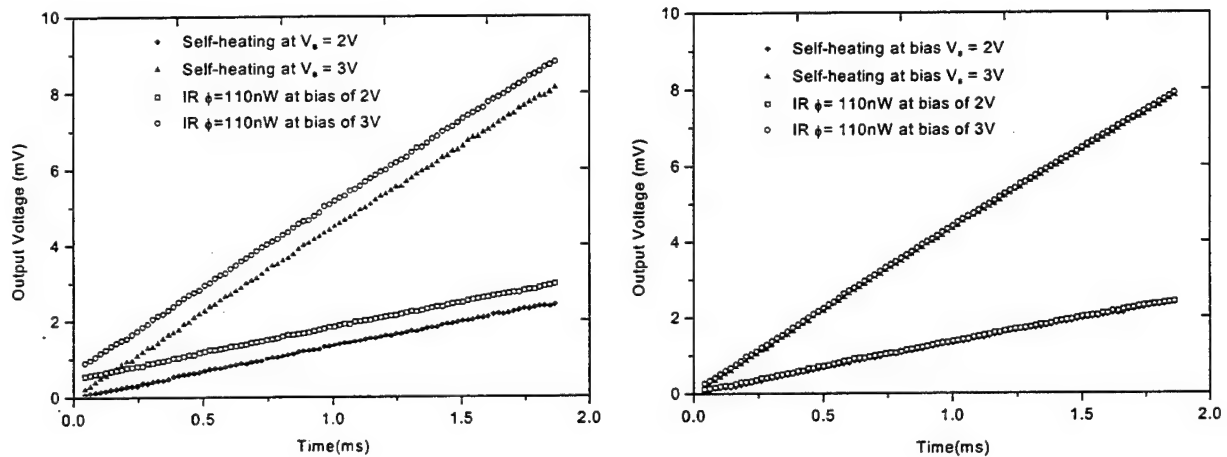


Figure III.8 Physical data for bolometer B₁ (left) and bolometer B₂ (right).

Once again, using bolometers with identical thermal characteristics, the following output voltage data is generated by PSPICE. (next page)

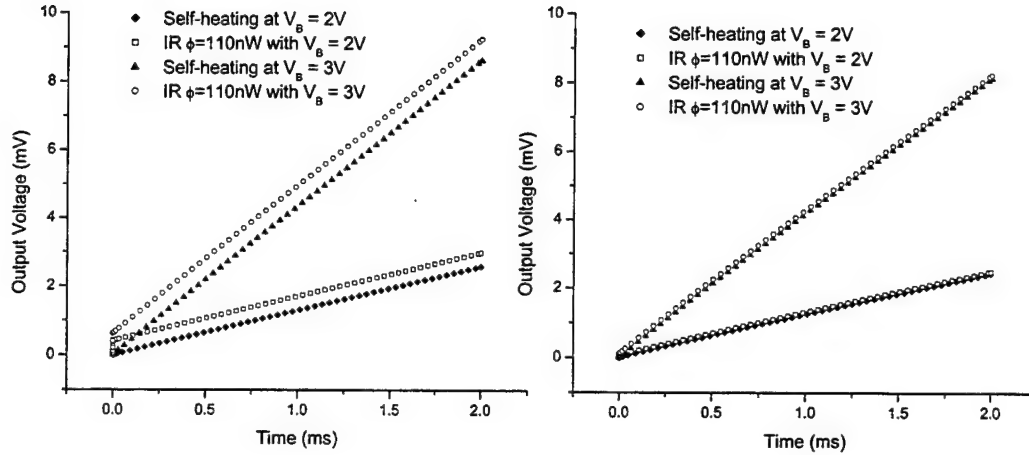


Figure III.9 PSPICE simulation of bolometer response to incident IR in addition to Joule heating. Bolometer B_1 is represented by the left graph, bolometer B_2 by the right graph.

In both figures III.8 and III.9, we can see the IR signal riding on top of the Joule heating signal. Additionally, the IR signal is significantly stronger on bolometer₁ than on bolometer₂, which was the goal of attempting to make bolometer₂ translucent to IR by increasing its thermal conductance. Nevertheless, because we are operating in the $dt \ll \tau$ region, the output voltages due to Joule heating for both bolometers are roughly equivalent, following the theory leading to equation (II.32). The PSPICE model appears quite accurate even at small transient times.

4. Modeling the Compensating Bolometer Wheatstone Bridge and Final Verification.

With the pieces in place and functioning properly, it remains to assemble the Wheatstone bridge with a compensating bolometer in place in order to cancel out the

majority of the Joule heating signal, leaving the IR signal and a roughly equivalent Joule heating signal as the input to the read-out circuitry, which would ostensibly begin with an amplifier (the very reason why it is advantageous to cancel out the enormous Joule heating signal). The following physical data show good cancellation of the Joule heating signal.

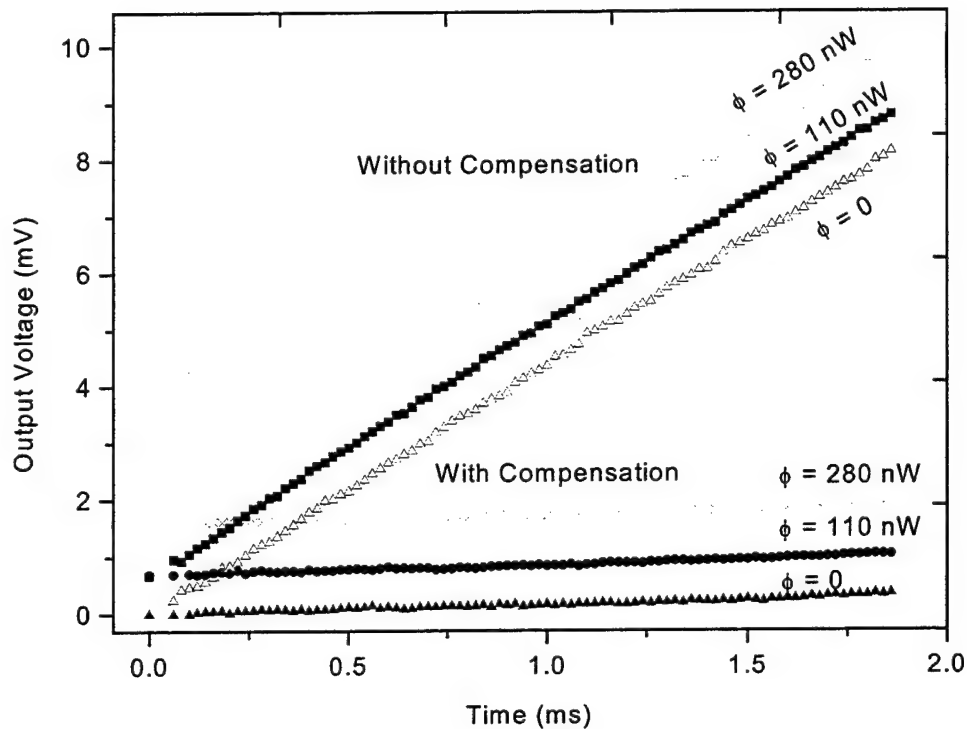


Figure III.10 IR and Joule heating response of the bridge consisting of two bolometers contrasted with response of the bolometer B_1 at bias voltage of 3V. The two bolometers were exposed to the same amount of infrared from a blackbody source.

The actual numerical physical data was not available, nor were the specifics of the experiment setup. For the PSPICE simulation, the Wheatstone bridge was set up with B_1 on one side with an equivalent resistor and B_2 on the other side with an equivalent

resistor. (This setup is shown in figure III.12.) The simulation yielded the following data.

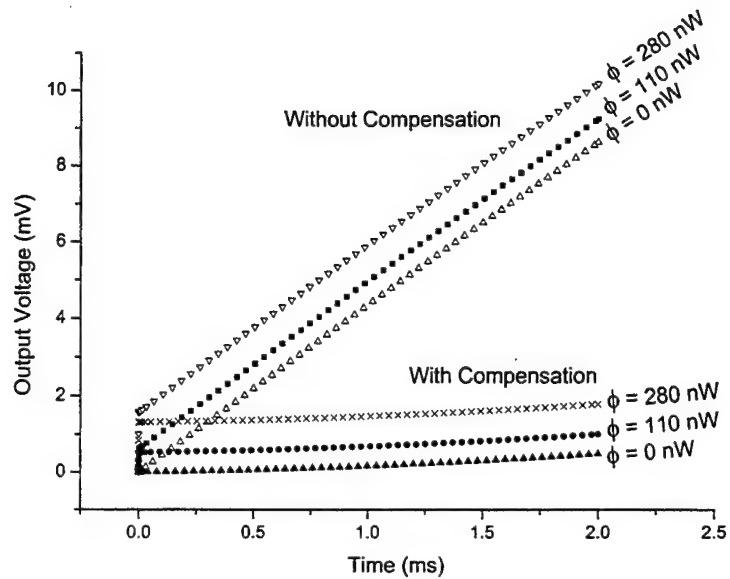


Figure III.11 PSPICE simulation of the IR and Joule heating response of the bridge consisting of two bolometers contrasted with response of the bolometer B_1 at bias voltage of 3V. The two bolometers were exposed to the same amount of simulated infrared flux from a blackbody source.

The correlation between the physical data and the simulation data is favorable, once again under 1% difference. Nevertheless, while the comparison of the physical cancellation with the simulated cancellation are inconclusive, the individual bolometers matched very well, and it is assumed that combining the two onto one compensated Wheatstone bridge should not alter their individual performance, as each is subject to the same voltage. Therefore, on the basis of the excellent correlation between reality and simulation as demonstrated by figures III.8 and III.9, the model is deemed a success.

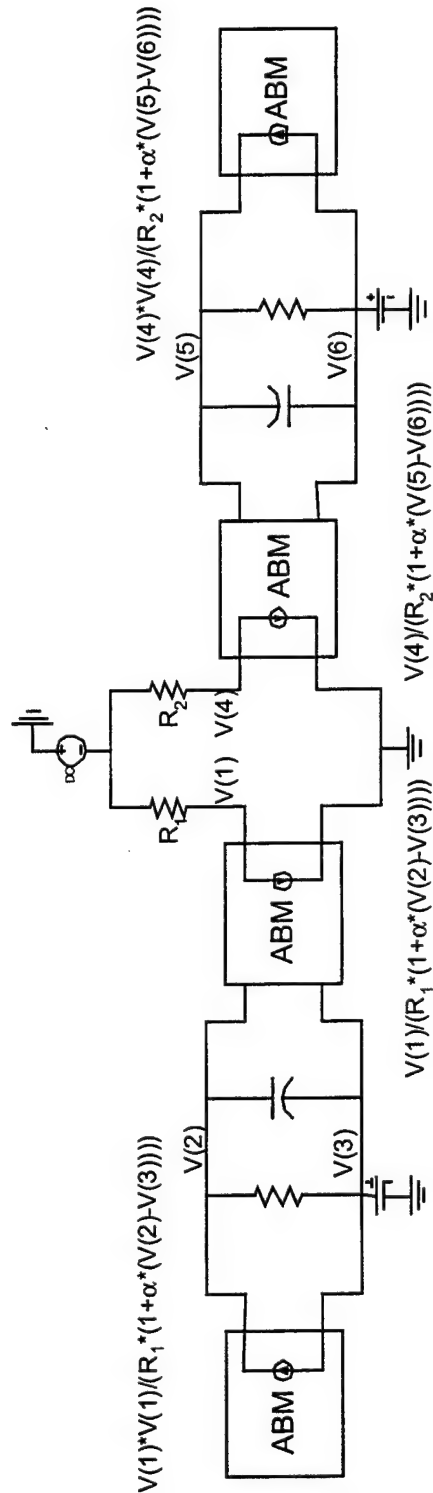


Figure III.12 Compensated bolometer Wheatstone bridge

[Note: to include variable thermal radiation for cases when the condition $\Delta T \ll T_0$ does not apply, ABM boxes should be generated in parallel in both bolometer circuits and programmed with the *Stefan-Boltzman Law*, equation (II.20).]

C. PARAMETRIC STUDY USING THE WHEATSTONE BRIDGE MODEL

The virtue of the PSPICE model can now be realized in that it is readily possible to conduct research and design studies of microbolometers without actually manufacturing them, saving time and money. Given a certain application, the designer may now quickly produce the necessary thermal characteristics required to design a useable device. It should be cautioned, however, that the assumptions and approximations made in designing the model must still hold true in order to create an accurate design. What follows is an example of how bolometer applications can be improved by employing the compensation technique, as illustrated through the use of the PSPICE model. The parameter to be used for comparison will be integration time, which therefore warrants a brief discussion.

1. Integration Time versus Noise Bandwidth

A cursory look at the forms of noise affecting bolometers reveals that they are dependent on frequency bandwidth Δf :

$$V_N^2 = 4kTR \cdot \Delta f \quad \text{Johnson noise}$$
$$V_f^2 = i^2 R^2 \left(B \frac{\Delta f}{f} \right) \quad 1/f \text{ noise}$$

where R is resistance, k is Boltzman's constant, T is temperature, and B is a constant for $1/f$ noise. (Shot noise is deemed negligible here). In our application, Δf is determined by the pulse width of the sampling pulse, where pulse width directly correlates to integration time t_{int} . Recalling from Fourier analysis, a narrower square pulse requires the addition of higher frequencies for its construction than a broader square pulse. Generally, the bandwidth is given by

$$\Delta f = \frac{1}{2 \cdot t_{\text{int}}} . \quad (\text{III.7})$$

Hence, the longer one can integrate a signal, the less noise will remain. In the comparison which follows, the decision is arbitrarily made that the signal will be integrated for a time period sufficient for the voltage response due to Joule heating to equal the voltage response due to an arbitrarily chosen IR radiation flux. This concept reflects the feasibility that the subsequent electronic subtraction of a Joule heating voltage on the same order of magnitude as the signal voltage reduces the probability of distorting the remaining signal voltage.

2. Application: Thermal Imaging Device

The necessity and usefulness of lightweight, portable thermal imaging devices are obvious to military, law enforcement and fire fighting personnel. The ability to image targets, suspects, and fires or hot spots in completely dark and/or smoky scenarios is critical to the success of many kinds of operations carried out by such personnel. As explained in the introduction, there are currently numerous devices available, but typically the operator must accept a trade-off in terms of sensitivity versus weight, because the more sensitive devices typically need to be cooled, which requires more power, weight and volume. The microbolometer fills this niche of high sensitivity and low weight/space at the expense of speed. Bolometers are relatively slow devices compared with many others, but this lack of speed really only precludes them from high-speed applications, such as IR warhead seekers.

Raytheon Systems Company has developed a prototype infrared imaging rifle-sight using an uncooled microbolometer focal plane array (FPA) (Radford, *et al*, 1998). (Implementation of the bolometer into a FPA is introduced in Appendix A.) This

system is typical for the kind of application needed in the Department of Defense. Because it is an integrated, micromachined chip technology, it is relatively low in cost compared with other microbolometer applications that require complicated manufacturing procedures to hide the reference bolometer from IR radiation, for example. In this case, the elemental structure is a one-bolometer Wheatstone bridge, and the Joule heating voltage is electronically subtracted using a dark current subtraction method. The thermal characteristics of the bolometer are given below.

Performance Parameter	Capability
Pixel Dimensions	50 (μm) ²
Thermal Conductance (G)	< 5×10^{-8} W/K
Thermal Capacity (H)	< 1×10^{-9} J/K
Thermal Time Constant (τ)	20 msec
α	> .02
Resistance (R_0)	50 k Ω

Table III.2 Raytheon IR imaging rifle-sight bolometer characteristics.

Given such a bolometer, we would like to determine the advantage gained in using a compensating bolometer in the Wheatstone bridge configuration. From equation (II.15) we see that the *saturation voltage* from a one-bolometer Wheatstone bridge is given by

$$V_{\text{saturation}} = \frac{V_b \cdot \alpha}{4} \frac{P}{G}. \quad (\text{III.8})$$

However, we must consider the saturation voltage for a Wheatstone bridge with an additional compensating bolometer, whose thermal conductance is different from the sensor bolometer by definition. This calculation would be analytically impossible were it not for the *principle of superposition* (Boas, 1983), which allows us to analyze the Wheatstone bridge twice, once each with a different bolometer, and then add the results. The principle of superposition is valid for any linear network containing resistors and

voltage sources. Using this method in the situation where the compensating bolometer is identical to the sensor bolometer with the exception of thermal conductance, we retrace the steps which lead to equation (II.15) and arrive at

$$V_{saturation} = \frac{V_b \cdot \alpha \cdot P}{4} \left(\frac{1}{G_1} - \frac{1}{G_2} \right). \quad (III.9)$$

A convenient figure of merit for the detector would be its signal response at 4 nW of incident IR flux. For the Raytheon bolometer circuit the signal would be 1.2 mV at $V_b=3$ V. For a reference bolometer with thermal conductance G_2 one order of magnitude greater (5×10^{-7} W/K), the signal would be 1.08 mV. There has been a 10% reduction in signal strength, and while the signal is certainly strong enough to manipulate, *any* reduction in signal strength is not desirable. However, the following graph illustrates the gain in integration time, assuming the signal will be integrated until the Joule heating matches the signal strength.

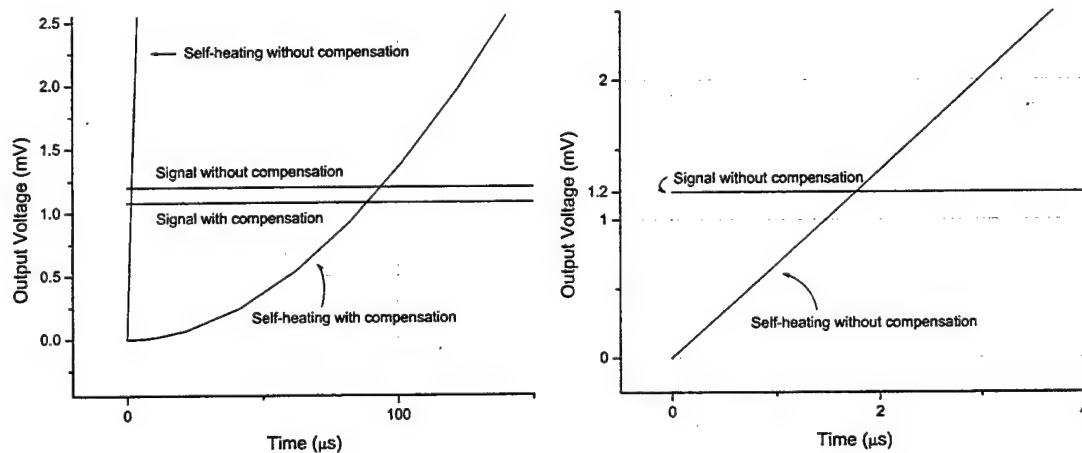


Figure III.13 Comparison of integration times with and without a compensating bolometer.

Clearly the benefit in integration time far outweighs this loss of signal strength, when one considers the effect on noise that an integration time of approximately two microseconds versus approximately ninety microseconds has. Following equation (III.7), the one bolometer circuit has a bandwidth of 5×10^5 Hz while the compensated circuit has a bandwidth of 1.1×10^4 Hz. It follows that the noise in the compensated bolometer is one-and-a-half orders of magnitude less than in the uncompensated circuit.

For imaging devices, this kind of noise reduction greatly enhances image quality. Video imagery is typically around 30 frames per second (fps), and even with the extended integration time we are nowhere near this limit. Even with the 10% loss of signal, implementation of a compensating bolometer in the IR imaging rifle-sight would improve it dramatically.

3. Further Possible Benefit – Cancellation by Integration

The benefit of having developed a working model of the compensated Wheatstone bridge becomes manifest when one simply begins to tinker with the design of the compensating bolometer. Instead of spending valuable resources in the design, manufacture and testing of physical bolometers, concepts can be modeled with ease. Such simulations may hold the key to the actual *elimination* of the Joule heating output voltage. In adjusting the thermal capacities and conductivities somewhat haphazardly, it was found that a Joule heating curve could be generated which first went negative, and then curved back positive before it exploded into the normal exponential growth curve. This was intriguing because it appeared to offer a means of canceling out the Joule heating voltage; simply integrating for a period long enough to cancel the negative voltage area with an equivalent positive voltage area would eliminate the Joule heating

voltage. Unfortunately, it was noted that adjusting the thermal mass of the reference bolometer would be very impractical in the micro-machining process, and therefore prohibitively expensive.

Fortunately, from the analytic description of the bolometer's early time response another option for achieving the same behavior appears:

$$V_{out} = \frac{V_b^3 \cdot \alpha}{16 \cdot R_0 \cdot H} \cdot t. \quad (II.19)$$

Equation (II.19) indicates that output voltage is equally dependent on the balancing resistor values as the thermal mass. This leads to the idea that the same advantageous output voltage curve can be generated by manipulating the value of R_0 on one side of the Wheatstone bridge. The figure below illustrates the idea.

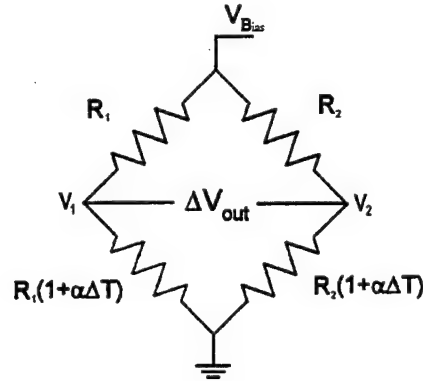


Figure III.14 Unbalanced Wheatstone bridge

The design shown in figure III.14 was implemented in PSPICE, with the same Raytheon bolometer as described by table III.2. This time, instead of precisely balancing R_1 and R_2 to equal each other, the value of R_2 was adjusted downward, resulting in the following set of output curves.

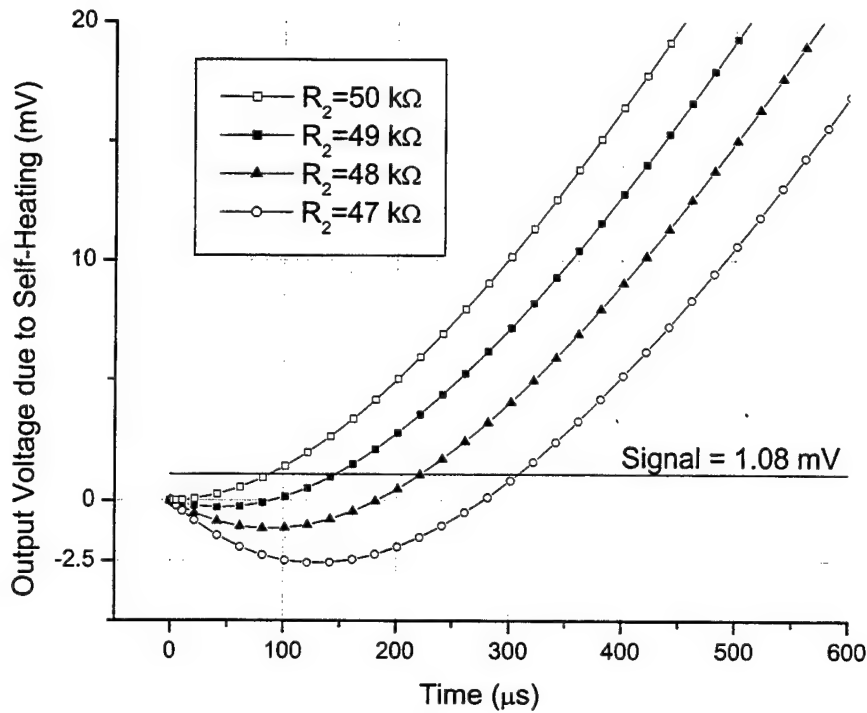


Figure III.15 PSPICE simulated output voltage versus time for integration by cancellation design.

As hoped for, adjusting R_2 lower than R_1 caused the curve to dip negative before launching exponentially in the positive direction. To integrate the Joule heating voltage, an integrator circuit, such as a Miller integrator, would have to be integrated into the pre-amplifier circuitry. It would therefore be important to keep the negative voltage dip roughly equivalent to the signal voltage, in order to keep the integrator's capacitor small enough for an appreciable output signal. R_2 meets this requirement, while providing for an integration time of approximately 450 microseconds. The Joule heating voltage could be entirely cancelled out, leaving behind only the signal voltage. Not only is the sensor greatly enhanced by removal of the Joule heating voltage, but the integration time has been extended, further improving the noise reduction by integration, and hence the

signal-to-noise ration (SNR). For example, the predominate source of noise, Johnson noise, may be calculated as follows.

Using the principle of superposition, we can derive the noise generated by each of the four resistors individually, and then add the noise figures in quadrature, as should be done with uncorrelated noise sources. Assuming all noiseless resistors with one noise voltage source for the lower right resistor, the circuit appears below.

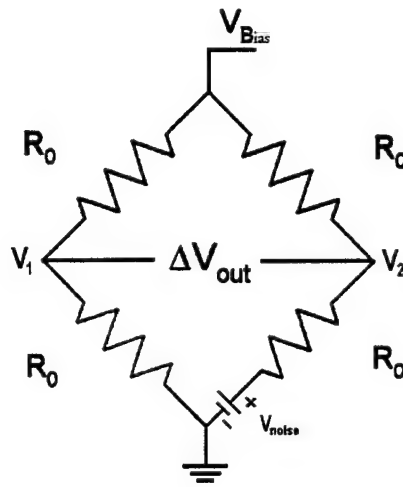


Figure III.16 Wheatstone bridge with voltage noise source for lower right resistor

The development is similar to that for equation (II.11), but this time V_2 is different, with

$$V_2 = \frac{V_b - V_n}{2} \quad (\text{III.10})$$

instead of $V_2 = \frac{V_b}{2}$, where V_n is the noise voltage due to one resistor. It then follows

that

$$\begin{aligned} \Delta V_{noise} &= |V_1 - V_2| = \frac{V_b}{2} - \frac{V_b - V_n}{2} \\ \Delta V_{noise} &= \frac{V_n}{2}. \end{aligned} \quad (\text{III.11})$$

For the total noise voltage, the individual noise voltages from each resistor are added in quadrature. In this case, the four individual noise voltages are equivalent, so

$$(V_{NOISE})^2 = 4 \times \left(\frac{V_n}{2} \right)^2$$

or

$$V_{NOISE} = V_n. \quad (III.12)$$

In dealing with Johnson noise,

$$V_{NOISE} = \sqrt{4kTR\Delta f}. \quad (III.13)$$

We may now evaluate the benefit of the longer integration time provided by the cancellation by integration technique. From figure III.9 we conservatively estimate an integration time of $\tau = 2 \mu s$, which also leaves behind 0.6 mV of Joule heating voltage.

Using this integration time, $R = 50 k\Omega$ and $T = 294 K$, equation (III.13) yields

$$V_{NOISE} = 14.25 \mu V. \quad (III.14)$$

Comparing this with cancellation by integration using $R_2 = 47 k\Omega$, we can estimate $\tau = 425 \mu s$ from figure II.11. This time equation (III.13) yields

$$V_{NOISE} = 0.98 \mu V. \quad (III.15)$$

In essence, these figures represent the minimum detectable signal threshold, because the sampling time is still short enough that $1/f$ noise is negligible compared to Johnson noise. In addition, the normally remaining Joule heating voltage can be completely eliminated, further reducing the inaccuracies that accompany electronic subtraction of the Joule heating voltage.

This appears to be a very promising technique, because, while altering an individual bolometer's thermal mass (H) is very difficult (requiring a three-dimensional architectural change), altering its thermal conductance (G) and baseline resistance is

simply a matter of changing the two-dimensional architecture of the reference bolometer in the micro-machining process.

THIS PAGE INTENTIONALLY LEFT BLANK

IV. CONCLUSION

By developing a working model on PSPICE, we have demonstrated the ability to explore more deeply the complex interaction between the thermal characteristics of the paired bolometers in the compensating Wheatstone bridge. Understanding the complex thermal interactions is only possible because the computer model numerically accounts for the higher-order terms which are neglected by necessity in analytic treatments. In practical terms, the model allows the researcher to tinker and to explore these interactions without incurring enormous costs or wasting valuable research time.

One example of the benefit of this kind of free tinkering was arrived at very quickly, with the discovery of cancellation by integration while using an unbalanced bridge. Previous thought had been entirely directed at the balanced bridge. Through the cancellation by integration technique developed in section III.C.3, we were able to realize a dramatic increase in integration time, which equated to a minimum detectable signal more than an order of magnitude smaller than without the technique.

A great deal of information awaits those who wish to more thoroughly explore the Wheatstone bridge arrangement using this model. With five independent variables all affecting the output voltage, there remain many unusual configurations worthy of study. One obviously worthwhile pursuit would be to study the sensitivity to manufacturing tolerances, in order to determine how tightly a particular design must be manufactured to deliver a tolerable performance. Another beneficial pursuit would be that of understanding the physical limits of a microbolometer based on the architectural design limits of the micromachining process (i.e., how narrow a bridge can be made and what this means in terms of thermal conductance limits).

THIS PAGE INTENTIONALLY LEFT BLANK

APPENDIX A: THE BOLOMETER ARRAY

A bolometer array can be designed with the reference bolometer outside of the pixel array. Using vertical and horizontal shift registers, each individual bolometer can be read sequentially and incorporated into the Wheatstone bridge structure in the lower right corner.

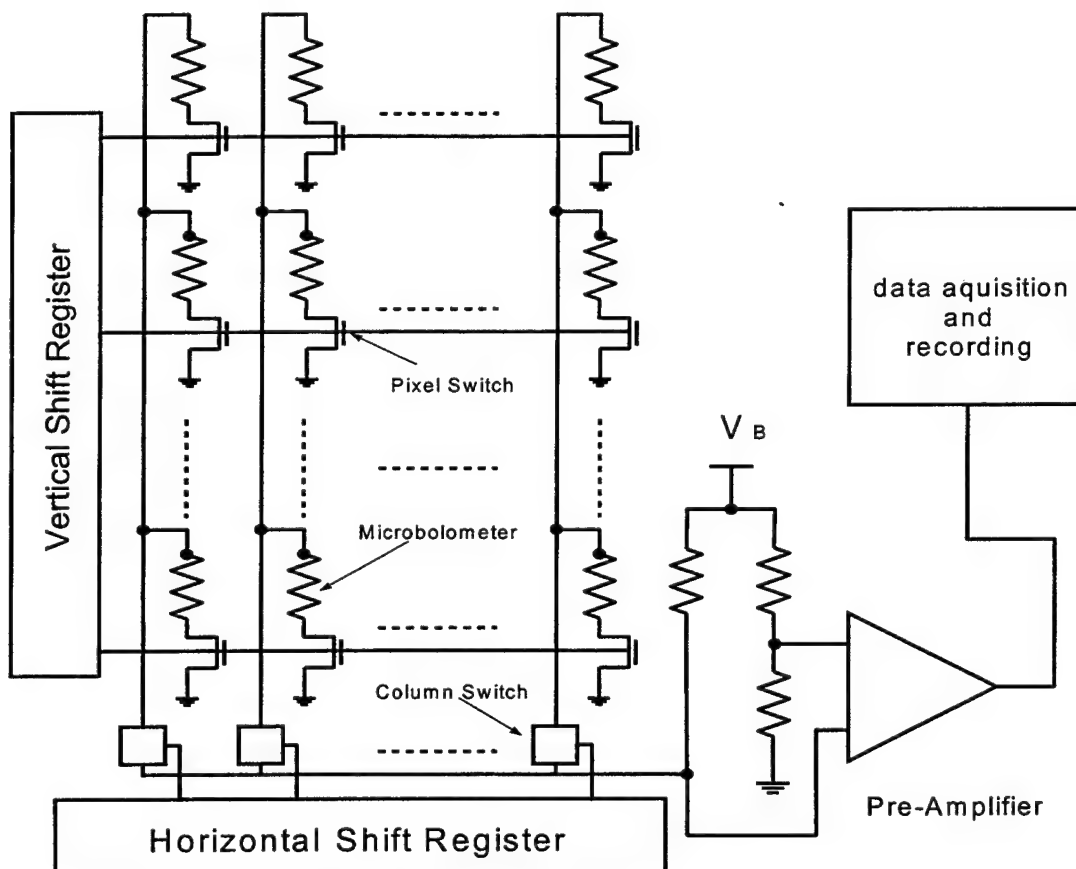


Figure A.1 Microbolometer Focal Plane Array (FPA) architecture.

THIS PAGE INTENTIONALLY LEFT BLANK

LIST OF REFERENCES

Boas, M., *Mathematical Methods in the Physical Sciences*, John Wiley and Sons, New York, New York, 1983.

Boreman, G., Dereniak, E., *Infrared Detectors and Systems*, John Wiley and Sons, New York, New York, 1996.

Gu, X., Karunasiri, G., Yu, G., Sridhar, U., Zeng, W., *On-chip compensation of self-heating effects in microbolometer detector arrays*, Sensors and Actuators, vol 69, pp. 92-96, 1998.

Haliday, D., Resnick, R., Walker, J., *Fundamentals of Physics, Extended*, Fifth Edition, John Wiley and Sons, New York, New York, 1997.

He, X., Karunasiri, G., Mei, T., Zeng, W., Neuzil, P., Sridhar, U., *Performance of Microbolometer Focal Plane Arrays Under Varying Pressure*, IEEE Electron Device Letters, vol. 21, no.5, pp. 233-235, 2000.

Karunasiri, G., Gu, X., Chen, G., Sridhar, U., *Extraction of thermal parameters of microbolometer infrared detectors using electrical measurement*, Proceedings of SPIE, vol. 3436, pp. 668-674, 1998.

Kimura, M., Kudo, T., European Patent # EP 0 798 545 A1, 1997

Kiran, R., Karunasiri, G., *Electro-thermal modeling of infrared microemitters using PSPICE*, Sensors and Actuators, vol 72, pp. 110-114, 1999.

Mori, T., Kudoh, T., Komatsu, K., Kimura M., *Vacuum-Encapsulated Thermistor Bolometer Type Miniature Infrared Sensor*, IEEE Electron Device Letters, # 0-7803-1833-1/94, pp. 257-262, 1994.

Radford, W., Wyles, J., Ray, M., Murphy, D., Kennedy, A., Finch, A., Moody, E., Cheung, F., Coda, R., Baur, S., *Microbolometer Uncooled Camera with 20 mK NETD*, Proceedings of SPIE, vol. 3436, pp. 668-674, 1998.

Ramakrishna, M., Karunasiri, G., Nuezil, P., Sridhar, U., Zeng, W., *Highly sensitive infrared temperature sensor using self-heating compensated microbolometers*, Sensors and Actuators, vol 79, pp. 122-127, 1999.

Rogalski, A., *New Trends in Semiconductor Infrared Detector*, Optical Engineering, 33, pp. 1395-1412, 1994.

Solymar, L., Walsh, D., *Electrical Properties of Materials*, Sixth Edition, Oxford University Press, New York, New York, 1998.

INITIAL DISTRIBUTION LIST

1. Defense Technical Information Center2
8725 John J. Kingman Road, Suite 0944
Ft. Belvoir, VA 22060-6218
2. Dudley Knox Library2
Naval Postgraduate School
411 Dyer Road
Monterey, CA 93943-5101
3. Gamani Karunasiri Code PH/Kg2
Department of Physics Department
Naval Postgraduate School
Monterey, CA 93943-5101
4. D. Scott Davis Code PH/Dv1
Department of Physics Department
Naval Postgraduate School
Monterey, CA 93943-5101
5. Chairman, Code PH1
Department of Physics Department
Naval Postgraduate School
Monterey, CA 93943-5101
6. Curricular Officer, Code 342
Engineering and Technology
Naval Postgraduate School
Monterey, CA 93943-5101
7. CDR (Ret) and Mrs. John B. Stetson, IV3
533 Water's Edge
Newtown Square, PA 19041